Axial flow effects on the stability of circular Couette flow with viscous heating

David L. Cotrell[a] and G. B. McFadden
Mathematical and Computational Sciences Division, National Institute of Standards and Technology, 100 Bureau Drive, Stop 8910, Gaithersburg, Maryland 20899-8910

(Received 24 June 2005; accepted 4 April 2006; published online 29 August 2006)

We consider flow between concentric circular cylinders driven jointly by a constant axial pressure gradient and rotation of one or both cylinder walls. In this work we account for viscous heating effects with a temperature-dependent viscosity, and have computed critical values with a radius ratio $\eta \equiv R_i/R_o = 0.827$ and rotation rate ratio $\kappa \equiv \Omega_o/\Omega_i = 0$ as used in the recent zero axial flow experiments of White and Muller [J. Fluid Mech. **462**, 133 (2002)], where R_i and R_o are the inner and outer cylinder radii, respectively, and Ω_i and Ω_o are the corresponding (signed) angular velocities. The effects of gravity are neglected, whereas conductivity, the volumetric coefficient of thermal expansion, density, and constant pressure specific heat are taken to be constant. The analysis extends previous results with no axial flow, and accounts for arbitrary disturbances of infinitesimal amplitude. Results show that over the entire range of axial flow rates considered, stability boundaries differ significantly from those found for the zero axial flow case. Consistent with the isothermal results of Cotrell, Rani, and Pearlstein [J. Fluid Mech. **509**, 353 (2004)] and the nonisothermal results of Cotrell and McFadden [Physics of Fluids **17**, 114102 (2005)], the critical disturbance is axisymmetric only over a finite range of Reynolds numbers beginning at zero, beyond which the critical disturbance becomes nonaxisymmetric. [DOI: 10.1063/1.2210938]

I. INTRODUCTION

Stability of steady, axisymmetric, incompressible flow driven by differential rotation of coaxial circular cylinders has been investigated extensively since the work of Taylor.[1] For this case, the flow becomes unstable due to an adverse radial distribution of angular momentum (i.e., centrifugal instability). Spiral Poiseuille flow, driven by cylinder rotation and an axial pressure gradient, has been of interest since the experiments of Cornish[2] and the theoretical work of Goldstein,[3] and is important in a number of applications. Papers by Takeuchi and Jankowski[4] and Ng and Turner[5] presented theoretical results concerning the stability of isothermal spiral Poiseuille flow with respect to nonaxisymmetric disturbances, and marked the beginning of a more complete understanding of its stability. More recently, Cotrell and Pearlstein[6] have shown how the centripetally driven instability connects, as conjectured by Reid[7] in the narrow-gap limit, to a nonaxisymmetric Tollmien-Schlichting-like instability of nonrotating annular Poiseuille flow at zero Taylor number. Here $\kappa = \Omega_o/\Omega_i$ is the angular velocity ratio, $\eta = R_i/R_o$ is the radius ratio, R_i and R_o are the inner and outer cylinder radii, respectively, and Ω_i and Ω_o are the corresponding (signed) angular speeds. For a comprehensive discussion of axial flow effects on the linear stability of isothermal circular Couette flow and comparison to experiment, see Cotrell and Pearlstein,[6] Cotrell *et al.*,[8] and references cited therein.

Previous work on the instability of nonisothermal circular Couette flow has largely focused on the effect of an imposed radial temperature gradient. When one considers the stability of circular Couette flow with a radial temperature gradient, instability can be due to either an adverse radial distribution of angular momentum (which was true for the isothermal case) or an adverse radial distribution of buoyancy due to an adverse temperature gradient (analogous to the thermal instability of a layer of fluid heated from below). The earliest theoretical work investigating the stability of circular Couette flow (i.e, no axial flow) with a radial temperature gradient (and thus considering the effects of an adverse radial distribution of buoyancy) is that of Yih,[9] Lai,[10] and Becker and Kaye,[11] in which the small-gap problem was considered. The first work to consider finite-sized gaps is that of Walowit *et al.*[12] in which they considered radius ratios of $\eta = 0.5$ and the limiting value $\eta \to 1$ for $\kappa = 0$, 0.2, and 0.25 (i.e., $\kappa = \eta^2$ for $\eta = 0.5$). Their work considers only axisymmetric disturbances, and the case in which the density is constant except when multiplying the centripetal acceleration term in the radial momentum equation (i.e., the Boussinesq approximation). For a given value of η, their results show that for a positive temperature difference between the cylinders (i.e., the outer cylinder is at a higher temperature than the inner cylinder), the critical Taylor number decreases with respect to its isothermal value as the difference in temperature increases. On the other hand, when the temperature difference is negative, the critical Taylor number increases as this difference becomes more negative. The bulk of the later work (with the exception of Ref. 13) has revisited the narrow gap case with axisymmetric disturbances.[14–17] The work of Kong and Liu[13] considers nonaxisymmetric disturbances for three radius ratios ($\eta = 0.95$, 0.8, and 0.5) and two rotation rate ratios ($\kappa = -1$ and 0.2) for the nonisothermal case. Their

[a]Present address: Lawrence Livermore National Laboratory, P.O. Box 808, Livermore, CA 94551.

results are consistent with those of Ref. 12 and show that for these combinations of κ and η, the value of the critical azimuthal disturbance varies with the magnitude and sign of the temperature difference between the cylinders.

More recently, Cotrell and McFadden[18] have investigated the effects of a radial temperature gradient on the linear stability of spiral Poiseuille flow (i.e., the base state is a superposition of circular Couette and annular Poiseuille flow). The effects of gravity are neglected, but the variation of density with temperature induces radial buoyancy effects through the centripetal acceleration term in the radial momentum equation. Their results show that for any $\kappa < \eta^2$ and a temperature gradient consistent with the Boussinesq approximation, the linear stability boundaries do not differ significantly from those found for the isothermal case[6] over the entire range of axial flow rates considered. On the other hand, for $\kappa > \eta^2$ and small axial flow rates, their results suggest that the flow is destabilized due to an adverse radial distribution of buoyancy for any positive temperature difference between the cylinder walls. This is in contrast to the isothermal results of Ref. 6 which show that there is no linear instability for axial flow rates below some minimum Reynolds number.

On the experimental side, Becker and Kaye[11] and Bjorklund and Kays[19] have considered gases, whereas Haas and Nissan[20] and Ho *et al.*[21] have considered liquids. The experiments of Ref. 11 investigate three cases of nonisothermal flow in an annulus using air as the working fluid. They first consider two unidirectional special cases, namely, axial and azimuthal flow, followed by the consideration of their combined effects. For the case of purely axial flow, they consider only Reynolds numbers well into the turbulent regime, whereas for purely rotational flow a wide range of Taylor numbers are considered. For the case of both axial and azimuthal flow, a wide range of rotation rate ratios and Reynolds numbers are considered. In the experiments of Ref. 19 for $0.80 < \eta < 0.95$ and $-1.96 \leqslant \kappa \leqslant 1$, the working fluid is air, the inner cylinder is heated, the outer cylinder is cooled, and there is no axial flow. In the experiments of Ref. 20 for $\eta \approx 0.857$, the working fluid is water, the inner cylinder is heated, the outer cylinder is cooled and fixed ($\kappa = 0$), and there is no axial flow.

On the other hand, buoyancy effects due to gravity may also produce axial flow, and have been considered in Refs. 22–24. In these studies, both experiments and computations have concentrated on the case in which the outer cylinder is fixed (i.e., $\kappa = 0$). Except for the axisymmetric calculations of Ref. 16 these studies have been primarily concerned with gravitational potentials. In these studies, results show that small imposed radial temperature gradients have a modest effect on the flow stability, with the critical Taylor number slightly increasing or decreasing depending on the magnitude of the Prandtl number and temperature difference between the cylinders. For a detailed summary of these studies see White and Muller.[25]

The stability of Newtonian flow in which the nonisothermal effects are due to viscous dissipation, rather than an imposed temperature difference, have received considerably less attention. Kolyshkin and Vaillancourt[26] have considered the linear stability analysis of flows with temperature gradients caused by uniform heat generation in the fluid. As was the case for the work of Chen and Kuo,[16] the fluid density is allowed to vary with temperature, and thus the temperature gradient causes buoyant secondary flows that ultimately lead to instability. In contrast to results for the case of differentially heated cylinders, the work of Kolyshkin and Vaillancourt[26] found that axisymmetric disturbances were the most unstable for small gap and small Prandtl number. For the most part, experimental and computational studies of nonisothermal Newtonian flows have focused on fluids that have low Prandtl numbers (less than approximately 100). More recently, Al-Mubaiyedh *et al.*[27,28] have performed linear stability calculations for fluids with much larger Prandtl numbers (approximately 11 000). Their work computes linear stability boundaries for the small-gap and fixed outer cylinder case, and considers both axisymmetric and nonaxisymmetric disturbances. Their results show that the critical Taylor number is greatly affected when viscous heating is taken into account. For the case of co-rotating cylinders (i.e., $\kappa > 0$), Thomas *et al.*[29] have performed linear stability calculations for axisymmetric disturbances over the range $0 \leqslant \kappa \leqslant 0.6$. These studies are particularly important in that destabilization is due to a temperature dependent viscosity without the inclusion of buoyancy, which has been found to be the driving force for nonisothermal destabilization of circular Couette flow in previous work. In Ref. 28 nonlinear stability calculations are also performed and results suggest that transition may be due to a subcritical instability. This work will be discussed in detail in Sec. III in the context of code validation.

Sukane *et al.*[30] performed experimental investigations into the effects of viscous heating in plane Couette flow, whereas Sukanek and Laurence[31] performed experimental investigations into the effects of viscous heating in circular Couette flow and Poiseuille flow in a circular cylinder. We note that a detailed review of the early literature on the effects of viscous heating on temperature and velocity profiles in simple flows can be found in these works. The results of Ref. 31 show that for circular Couette flow, the stress goes through a maximum with increasing shear rate. Sukanek and Laurence[31] also report results that suggest an instability related to viscous heating in circular Poiseuille flow. More recently, White and Muller[25,32] have considered $\eta = 0.827$ and 0.912 for nonzero κ, where their range of κ is similar to the computational work in Ref. 29. The zero axial flow experimental results in Refs. 25 and 32 are discussed in detail in Refs. 28 and 29 and thus will not be treated in detail here.

Here, we report linear stability boundaries for $\eta = 0.827$ and $\kappa = 0$. The results account for arbitrary disturbances of infinitesimal amplitude, and cover a wide range of temperatures and axial flow rates. In this analysis we will neglect the effect of gravity. We note that it is extremely important to consider viscous heating in hydrodynamic stability calculations and experiments, because unlike externally imposed temperature gradients, viscous heating is a strong function of the fluid properties and cannot be easily controlled or eliminated. We know of no previous computations or experiments

that consider axial flow effects on the linear stability of circular Couette flow with viscous heating.

The problem is formulated in Sec. II, followed by a description of the numerical approach in Sec. III. Results and discussion are presented in Secs. IV and V, respectively, and conclusions are presented in Sec. VI.

II. FORMULATION

We consider flow between concentric circular cylinders held at the same constant temperature (i.e., $T_i=T_o$) driven jointly by a constant axial pressure gradient and rotation of one or both cylinders, where T_i and T_o are the temperatures of the inner and outer cylinders, respectively. We choose an inertial frame in which the cylinders have no axial velocity. The governing equations are nondimensionalized using the dimensionless radial coordinate $r=R/d$, axial coordinate $z=Z/d$, time $\tau=t\Omega_i R_i/d$, pressure $p=P/(\rho_r\Omega_i^2R_i^2)$, temperature $\Theta=T/T_r$, and velocity $v=V/(\Omega_i R_i)$, where $d=R_o-R_i$ is the difference between the outer and inner radii, respectively, Ω_i is the angular velocity of the inner cylinder, and ρ_r is the density evaluated at the reference temperature (T_r) used in the fluid property correlations. In this work, we take the fluid to be glycerin and allow the fluid properties to vary with temperature (see Table I). The temperature dependence of the fluid properties is taken from the experimental work of Ref. 32. The dimensionless continuity, momentum, and energy equations are

TABLE I. Temperature dependence of the fluid properties for glycerin, based on the reference temperature $T_r=298$ K.

Physical property	Temperature dependence	Value at $T_r=298$ K
μ (kg/ms)	$\mu=\mu_r\exp\left[7.31\times10^3\left(\frac{1}{T}-\frac{1}{T_r}\right)\right]$	0.995
	$=\mu_r\exp\left[\epsilon_1\left(\frac{1}{\Theta}-1\right)\right]$	
	$=\mu_r\exp\left[24.53\left(\frac{1}{\Theta}-1\right)\right]$	
ρ (kg/m^3)	$\rho=\rho_r-0.561(T-T_r)$	1257
	$=\rho_r[1+\epsilon_2(\Theta-1)]$	
	$=\rho_r[1-0.133(\Theta-1)]$	
c_P (J/kg K)	$c_P=c_{\mathrm{Pr}}+6.43(T-T_r)$	2417
	$=c_{\mathrm{Pr}}[1+\epsilon_3(\Theta-1)]$	
	$=c_{\mathrm{Pr}}[1+0.793(\Theta-1)]$	
k (W/mK)	$k=$constant	0.285
α (K^{-1})	$\alpha=$constant	4.5×10^{-4}

$$\epsilon_2\frac{D\Theta}{D\tau}+[1+\epsilon_2(\Theta-1)]\left[\frac{1}{r}\frac{\partial}{\partial r}(rv_r)+\frac{1}{r}\frac{\partial v_\theta}{\partial\theta}+\frac{\partial v_z}{\partial z}\right]=0, \tag{1a}$$

$$(1-\epsilon_2\Theta-\epsilon_2)\left[\frac{Dv_r}{D\tau}-\frac{v_\theta^2}{r}\right]=-\frac{\partial p}{\partial r}+\frac{f}{\mathrm{Ta}_r}\left[\nabla^2 v_r-\frac{v_r}{r^2}-\frac{2}{r^2}\frac{\partial v_\theta}{\partial\theta}\right]+\frac{2}{\mathrm{Ta}_r}\frac{\partial f}{\partial\Theta}\frac{\partial\Theta}{\partial r}\frac{\partial v_r}{\partial r}+\frac{1}{\mathrm{Ta}_r}\frac{1}{r}\frac{\partial f}{\partial\Theta}\frac{\partial\Theta}{\partial\theta}\left[r\frac{\partial}{\partial r}\left(\frac{v_\theta}{r}\right)+\frac{1}{r}\frac{\partial v_r}{\partial\theta}\right]+\frac{1}{\mathrm{Ta}_r}\frac{\partial f}{\partial\Theta}\frac{\partial\Theta}{\partial z}\left[\frac{\partial v_z}{\partial r}+\frac{\partial v_r}{\partial z}\right], \tag{1b}$$

$$(1-\epsilon_2\Theta-\epsilon_2)\left[\frac{Dv_\theta}{D\tau}+\frac{v_\theta v_r}{r}\right]=-\frac{1}{r}\frac{\partial p}{\partial\theta}+\frac{f}{\mathrm{Ta}_r}\left[\nabla^2 v_\theta-\frac{v_\theta}{r^2}+\frac{2}{r^2}\frac{\partial v_r}{\partial\theta}\right]+\frac{1}{\mathrm{Ta}_r}\frac{\partial f}{\partial\Theta}\frac{\partial\Theta}{\partial r}\left[r\frac{\partial}{\partial r}\left(\frac{v_\theta}{r}\right)+\frac{1}{r}\frac{\partial v_r}{\partial\theta}\right]+\frac{2}{\mathrm{Ta}_r}\frac{1}{r}\frac{\partial f}{\partial\Theta}\frac{\partial\Theta}{\partial\theta}\left[\frac{1}{r}\frac{\partial v_\theta}{\partial\theta}+\frac{v_r}{r}\right]+\frac{1}{\mathrm{Ta}_r}\frac{\partial f}{\partial\Theta}\frac{\partial\Theta}{\partial z}\left[\frac{\partial v_\theta}{\partial z}+\frac{1}{r}\frac{\partial v_z}{\partial\theta}\right], \tag{1c}$$

$$(1-\epsilon_2\Theta-\epsilon_2)\frac{Dv_z}{D\tau}=-\frac{\partial p}{\partial z}+\frac{f}{\mathrm{Ta}_r}\nabla^2 v_z+\frac{1}{\mathrm{Ta}_r}\frac{\partial f}{\partial\Theta}\frac{\partial\Theta}{\partial r}\left[\frac{\partial v_z}{\partial r}+\frac{\partial v_r}{\partial z}\right]+\frac{1}{\mathrm{Ta}_r}\frac{1}{r}\frac{\partial f}{\partial\Theta}\frac{\partial\Theta}{\partial\theta}\left[\frac{\partial v_\theta}{\partial z}+\frac{1}{r}\frac{\partial v_z}{\partial\theta}\right]+\frac{2}{\mathrm{Ta}_r}\frac{\partial f}{\partial\Theta}\frac{\partial\Theta}{\partial z}\frac{\partial v_z}{\partial z}, \tag{1d}$$

$$[1+\epsilon_2(\Theta-1)+\epsilon_3(\Theta-1)+\epsilon_2\epsilon_3(\Theta-1)]\frac{D\Theta}{D\tau}=\frac{1}{\mathrm{Pr}_r\mathrm{Ta}_r}\nabla^2\Theta+\frac{2\mathrm{Br}_r f}{\mathrm{Pr}_r\mathrm{Ta}_r}\left\{\left[\frac{\partial v_r}{\partial r}\right]^2+\left[\frac{1}{r}\frac{\partial v_\theta}{\partial\theta}+\frac{v_r}{r}\right]^2+\left[\frac{\partial v_z}{\partial z}\right]^2\right\}+\frac{\mathrm{Br}_r f}{\mathrm{Pr}_r\mathrm{Ta}_r}\left\{\left[\frac{\partial v_\theta}{\partial z}+\frac{1}{r}\frac{\partial v_z}{\partial\theta}\right]^2+\left[\frac{\partial v_z}{\partial r}+\frac{\partial v_r}{\partial z}\right]^2+\left[\frac{1}{r}\frac{\partial v_r}{\partial\theta}+r\frac{\partial}{\partial r}\left(\frac{v_\theta}{r}\right)\right]^2\right\}, \tag{1e}$$

where

$$\frac{D}{D\tau}=\frac{\partial}{\partial\tau}+v_r\frac{\partial}{\partial r}+\frac{v_\theta}{r}\frac{\partial}{\partial\theta}+v_z\frac{\partial}{\partial z},$$

$$\nabla^2=\frac{1}{r}\frac{\partial}{\partial r}\left(r\frac{\partial}{\partial r}\right)+\frac{1}{r^2}\frac{\partial^2}{\partial\theta^2}+\frac{\partial^2}{\partial z^2},$$

and $f=\exp[\epsilon_1(1/\Theta-1)]$, $\epsilon_1=|(T/\mu)(\partial\mu/\partial T)|_{T_r}$ is the dimensionless activation energy, ϵ_2 is the dimensionless slope of the density function, and ϵ_3 is the dimensionless slope of the constant pressure specific heat function. These parameters characterize the thermal sensitivity of the viscosity, density, and constant pressure specific heat, respectively. We note that setting $\epsilon_2=0$ results in the constant density case, whereas setting $\epsilon_3=0$ represents the case with constant pressure specific heat.

The dimensionless parameters, based on fluid properties evaluated at the reference temperature T_r, are the Taylor number $\mathrm{Ta}_r=\Omega_i R_i d\rho_r/\mu_r$, the Brinkman number $\mathrm{Br}_r=\mu_r(\Omega_i R_i)^2/kT_r$, the Prandtl number $\mathrm{Pr}_r=c_{\mathrm{Pr}}\mu_r/k$, and the Reynolds number $\mathrm{Re}_r=V_{zr}d\rho_r/\mu_r$ (which shows up in the base state), where μ_r is the dynamic viscosity, k is the thermal conductivity (taken to be a constant in this work), c_{Pr} is the constant pressure specific heat, and $V_{zr}=[(\partial P/\partial z)d/\rho_r]^{1/2}$ is a characteristic axial velocity based on the axial pressure gradient, all evaluated at the reference temperature. As we are allowing the fluid viscosity to vary with temperature, the effect of the viscosity gradient can be accounted for through the Nahme number, $\mathrm{Na}_r=\epsilon_1\mathrm{Br}_r$. The Nahme number represents the maximum fractional change in the viscosity under the action of viscous heating. It has been shown by Pearson[33] that the Nahme number works well in characterizing the coupling between the momentum and energy equations.

To compare to previous experimental and computational results (e.g., Refs. 25, 28, 29, and 32) for $\mathrm{Re}_r=0$, we define versions of the dimensionless parameters rescaled by the inner cylinder temperature T_i. The relevant rescaled dimensionless parameters are the Reynolds number $\mathrm{Re}_i=V_{zi}d\rho_i/\mu_i$, the Prandtl number $\mathrm{Pr}_i=c_{Pi}\mu_i/k$, the Taylor number $\mathrm{Ta}_i=\Omega_i R_i d\rho_i/\mu_i$, and the Nahme number $\mathrm{Na}_i=\epsilon_1\mathrm{Br}_i$. Here all fluid properties have been evaluated at T_i. We note that this scaling will be used in the current work to discuss and represent the results (see Sec. IV).

A. Base state

The dimensionless steady, axisymmetric, and axially fully developed equations governing the base state are

$$f\left[\frac{\partial^2 v_{\theta b}}{\partial r^2}+\frac{1}{r}\frac{\partial v_{\theta b}}{\partial r}-\frac{v_{\theta b}}{r^2}\right]+\frac{\partial f}{\partial\Theta_b}\frac{\partial\Theta_b}{\partial r}\left[\frac{\partial v_{\theta b}}{\partial r}-\frac{v_{\theta b}}{r}\right]=0, \tag{2a}$$

$$f\left[\frac{\partial^2 v_{zb}}{\partial r^2}+\frac{1}{r}\frac{\partial v_{zb}}{\partial r}\right]+\frac{\partial f}{\partial\Theta_b}\frac{\partial\Theta_b}{\partial r}\frac{\partial v_{zb}}{\partial r}=\frac{\mathrm{Re}_r^2}{\mathrm{Ta}_r}, \tag{2b}$$

$$\frac{\partial^2\Theta_b}{\partial r^2}+\frac{1}{r}\frac{\partial\Theta_b}{\partial r}+\mathrm{Br}_r f\left(\frac{\partial v_{zb}}{\partial r}\right)^2+\mathrm{Br}_r f\left[\left(\frac{\partial v_{\theta b}}{\partial r}\right)^2-\frac{2v_{\theta b}}{r}\frac{\partial v_{\theta b}}{\partial r}+\frac{v_{\theta b}^2}{r^2}\right]=0, \tag{2c}$$

where we assume no-slip and constant temperature on the rigid inner and outer walls at $r=\eta/(1-\eta)$ and $1/(1-\eta)$, respectively,

$$v_{\theta b}(r_i)=1, \tag{3a}$$

$$v_{\theta b}(r_o)=\frac{\kappa}{\eta}, \tag{3b}$$

$$v_{zb}(r_i)=0, \tag{3c}$$

$$v_{zb}(r_o)=0, \tag{3d}$$

$$\Theta_b(r_i)=\frac{T_i}{T_r}, \tag{3e}$$

$$\Theta_b(r_o)=\frac{T_o}{T_r}. \tag{3f}$$

We note that the numerical method used in solving for the base state is identical to that used to solve the linear stability problem. Thus, we postpone discussion of the numerical method until Sec. III.

B. Linear stability

In order to investigate the linear stability of the base state, we write the dimensionless velocity, pressure, and temperature as a linear sum of the base state plus a small perturbation

$$v=v_b+\delta v', \tag{4a}$$

$$p=p_b+\delta p', \tag{4b}$$

$$\Theta=\Theta_b+\delta\Theta', \tag{4c}$$

where $|\delta|\ll 1$. In order to linearize the system about the base state, one substitutes (4) into (1) and keeps the terms of order δ. The disturbance velocity (v'), pressure (p'), and temperature (Θ') fields in normal mode form are

$$\begin{bmatrix} v'(r,\theta,z,\tau)\\ p'(r,\theta,z,\tau)\\ \Theta'(r,\theta,z,\tau)\end{bmatrix}=\begin{bmatrix}\tilde{v}(r)\\ \tilde{p}(r)\\ \tilde{\Theta}(r)\end{bmatrix}\exp[i(az+m\theta)+\sigma\tau], \tag{5}$$

where a, m, and $\sigma=\sigma_r+i\sigma_i$ are the axial wave number, azimuthal wave number, and temporal eigenvalue, respectively; we take a to be real, m to be an integer, and σ to be complex. At order δ we obtain a system of homogeneous linear ordinary differential equations in the radial coordinate for the disturbance velocity components ($\tilde{v}$), pressure ($\tilde{p}$), and temperature ($\tilde{\Theta}$) eigenfunctions.

III. NUMERICAL APPROACH

A. Base state

We note that the equations governing the base state (2) are extremely nonlinear. Because the fluid viscosity is related to temperature by an Arrhenius relationship, the system has coefficients that depend exponentially on the inverse temperature. This problem is related to the circular Poiseuille flow work of Kearsley,[34] and to the more recent annular Couette flow work of Kearsley,[35] where viscosity depends exponentially on temperature. Their work differs from the current study in that we consider both types of forcing simultaneously, and assume an Arrhenius relationship between viscosity and temperature. To the best of our knowledge, we know of no closed form solution to the system (2). Thus we take a numerical approach to the solution of (2), namely a pseudospectral discretization in Chebyshev polynomials. We discretize the base state equations by collocation, using N_p^b Chebyshev polynomials to represent the velocity components and temperature. The momentum and energy equations are collocated at N_p^b-2 interior Gauss-Lobatto points. The boundary conditions are satisfied explicitly, giving a quadratically nonlinear algebraic system of dimension $3N_p^b$, which is solved by Newton iteration. As an initial iterate, we use the nonisothermal base state solution of Ref. 18. If needed, converged solutions at one spatial resolution can be interpolated using a prolongation operator to get an initial iterate for the next-higher resolution.

We also note that results for the system (2) have not been shown before (even for the limiting case of $\mathrm{Re}_i=0$), so we present results for values of Θ_i and Re_i spanning the range considered in the linear stability analysis (see Sec. IV). The parameter values (i.e., $\overline{\mathrm{Ta}_i}$ and $\overline{\mathrm{Br}_i}$) used to compute the base state in this section are chosen to be near critical values found for $m=0$ in the linear stability analysis for a given Θ_i and Re_i (again see Sec. IV). Figures 1(a)–1(c) show $v_{\theta b}$, v_{zb}, and Θ_b vs r for $\eta=0.827$, $\kappa=0$, $\Theta_i=0.95$ and $\mathrm{Re}_i=0$ (solid curve), $\mathrm{Re}_i=50$ (dashed curve), and $\mathrm{Re}_i=100$ (dotted curve). As shown in Fig. 1(a), $v_{\theta b}$ begins to depart from its nearly linear dependence on r as Re_i increases beyond zero. As Re_i grows large, $v_{\theta b}$ becomes more and more signoidal in nature, and one would expect to see the change in $v_{\theta b}$ near the inflection point grow sharper as Re_i grows large. This change in $v_{\theta b}$ is caused by increased viscous heating brought about by the increase in axial shear due to increases in axial flow. As can be seen in Fig. 1(b), the maximum of v_{zb} initially increases sublinearly with Re_i. In contrast to trends in v_{zb}, Fig. 1(c) shows that the maximum of Θ_b increases almost linearly with Re_i. As expected, increases in the temperature field due to viscous heating are much larger for nonzero Re_i [see Fig. 1(c)]. Figures 2(a)–2(c) show $v_{\theta b}$, v_{zb}, and Θ_b vs r for $\eta=0.827$, $\kappa=0$, $\Theta_i=1.08$ and $\mathrm{Re}_i=0$ (solid curve), $\mathrm{Re}_i=50$ (dashed curve), and $\mathrm{Re}_i=100$ (dotted curve). In contrast to the results for $\Theta_i=0.95$ [Fig. 1(a)], Fig. 2(a) shows that it takes a much larger axial flow rate to modify $v_{\theta b}$ significantly at higher temperatures. This is because viscous terms in the momentum equations become less important at higher temperatures due to the fact that f gets small as Θ_i gets large. As can be seen in Fig. 2(b), the maximum of v_{zb} initially increases superlinearly with Re_i. This behavior differs significantly from what we saw for $\Theta_i=0.95$ [see Fig. 1(b)]. In contrast to trends in v_{zb}, Fig. 2(c) shows that the maximum of Θ_b increases sublinearly with Re_i. We note that due to our assumed relationship between temperature and viscosity, the maximum effects of variable viscosity on the temperature field are seen at low temperatures.

B. Linear stability analysis

We also discretize the disturbance equations by collocation, using N_p^s Chebyshev polynomials to represent the disturbance velocity components and temperature and N_p^s-1 Chebyshev polynomials for the pressure. The momentum and energy equations are collocated at N_p^s-2 interior Gauss-Lobatto points, whereas the continuity equation is collocated at N_p^s-1 interior Gauss points. The boundary conditions are satisfied explicitly, giving a generalized matrix eigenvalue problem of dimension $5N_p^s-1$, whose temporal eigenvalues $\sigma=\sigma_r+i\sigma_i$ are found using the software package LAPACK (or the sparse eigenvalue solver ARPACK as discussed in the following). In this work, we use the shear rate, $\dot{\gamma}$, as the bifurcation parameter (as was also done in Ref. 28). In order to accomplish this, we rewrite the Taylor number $\mathrm{Ta}_r=\dot{\gamma}[(\rho_r d^2)/\mu_r]$ and the Brinkman number $\mathrm{Br}_r=\dot{\gamma}^2[(\mu_r d^2)/(kT_r)]$ in terms of $\dot{\gamma}$.

For given Re_i, Θ_i, κ, and η, we seek minimum values of $\dot{\gamma}$, for which at least one temporal eigenvalue has $\sigma_r=0$ for some m and a, and all other σ lie in the left half-plane for all m and a. As discussed for both isothermal and nonisothermal cases in previous work,[4–6,18,36] analysis can be restricted to $a\geqslant 0$ without loss of generality as long as one takes into account both positive and negative values of the azimuthal wave number.

To compute critical values of $\dot{\gamma}$, we begin with approximately 300 discrete axial wave numbers nonuniformly distributed over $0<a\leqslant 50$. For each m considered (*vide infra*), we do "axial wave number traverses" at fixed $\dot{\gamma}$, until we locate a value ($\dot{\gamma}_s$) stable at each of the wave numbers (in the discrete list) and another ($\dot{\gamma}_u$) unstable for at least one a. For each of $\dot{\gamma}_s$ and $\dot{\gamma}_u$, we identify the a_j, among the discrete list of values considered, at which σ_r assumes its maximum, and fit a quadratic through the points (σ_r,a), with $a=a_{j-1}$, a_j, and a_{j+1}. Differentiating, we estimate a maximizing σ_r at $\dot{\gamma}_s$ and $\dot{\gamma}_u$, and use this process to iteratively refine a at each $\dot{\gamma}$ until $|1-\sigma_{r,n+1}^{\max}/\sigma_{r,n}^{\max}|<1\times10^{-6}$. Once maximum values of σ_r (negative for $\dot{\gamma}_s$ and positive for $\dot{\gamma}_u$) and the corresponding a are found, secant iteration between $\dot{\gamma}_s$ and $\dot{\gamma}_u$ is used to estimate a new $\dot{\gamma}_1$ at which σ_r^{max} vanishes. A wave number traverse at $\dot{\gamma}_1$ gives the sign of $\sigma_r^{\max}$, which determines whether $\dot{\gamma}_1$ replaces $\dot{\gamma}_s$ or $\dot{\gamma}_u$. Secant iteration is continued until $|1-\dot{\gamma}_{q+1}/\dot{\gamma}_q|<1\times10^{-6}$. (Requiring convergence of $|1-\dot{\gamma}_s/\dot{\gamma}_u|$ gave indistinguishable stability boundaries.) At this juncture, for each m we have one or more extremal values of $\dot{\gamma}$ and associated values of a. For each m, such a $(a,\dot{\gamma})$ pair corresponds to an extremum on a neutral curve (i.e., a curve in the a-$\dot{\gamma}$ or the corresponding a-Ta_i plane). We note that a neutral curve is a curve dividing portions of the a-Ta_i plane in which no temporal eigenvalue lies in the right

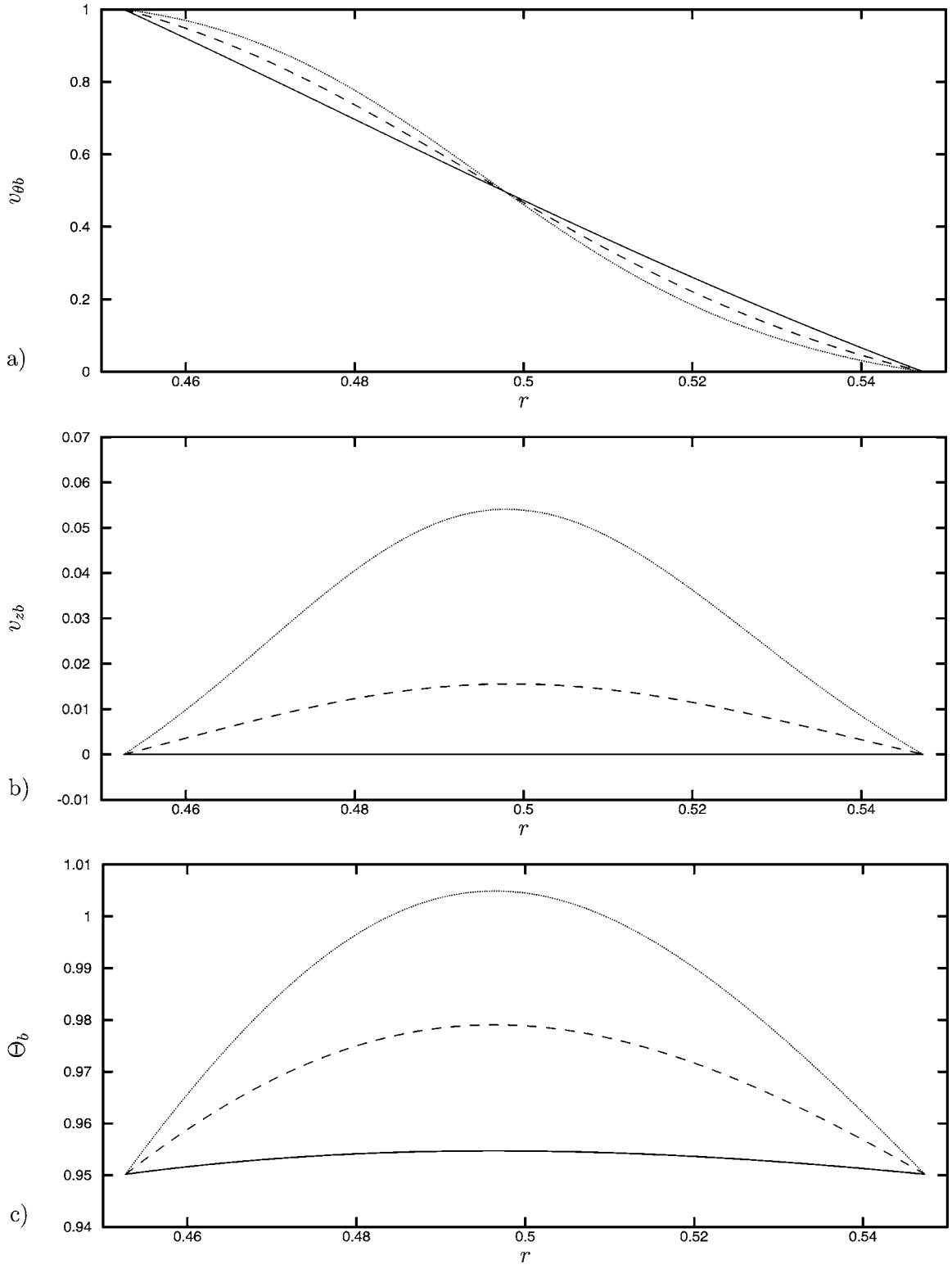

FIG. 1. For $\epsilon_2=\epsilon_3=0$, $\kappa=0$, $\eta=0.827$, $\Theta_i=0.95$, and $\mathrm{Re}_i=0$ (solid), 50 (dashed), and 100 (dotted): (a) $v_{\theta b}$, (b) v_{zb}, (c) Θ_b vs r.

half-plane (RHP), from portions in which one or more eigenvalues lie in the RHP. The corresponding neutral curve extremum values of the Taylor number, axial wave number, axial wave speed, and Nahme number are defined as $\overline{\mathrm{Ta}}_i$, $\bar{a}$, $\bar{c}$, and $\overline{\mathrm{Na}}_i$, respectively [shown as dotted curves in Figs. 3(a)–3(d), 5(a)–5(d), and 7(a)–7(d) of Sec. IV for the corresponding value of m].

The critical azimuthal wave number (m_{crit}) is the value of m for which $\overline{\mathrm{Ta}}_i$ assumes its minimum over the range of m considered for a given value of Re_i and Θ_i. The corresponding critical axial wave number and axial wave speed are denoted by $\bar{a}_{\mathrm{crit}}$ and $\bar{c}_{\mathrm{crit}}=\sigma_{i,\mathrm{crit}}/\bar{a}_{\mathrm{crit}}$, respectively. Once we know the critical shear rate, we can compute the critical Prandtl number $\overline{\mathrm{Pr}}_{i,\mathrm{crit}}$, the critical Nahme number $\overline{\mathrm{Na}}_{i,\mathrm{crit}}$, and

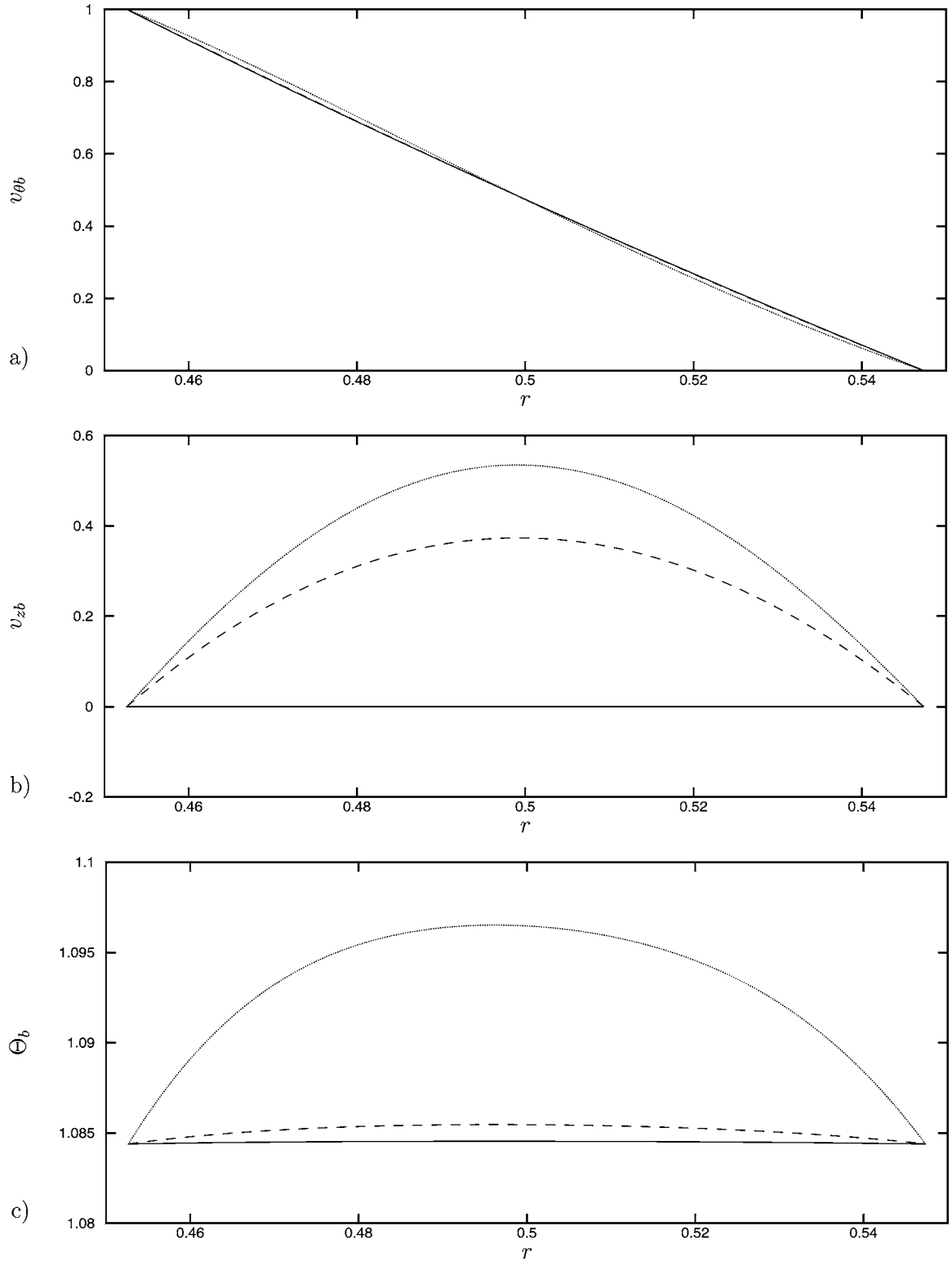

FIG. 2. For $\epsilon_2=\epsilon_3=0$, $\kappa=0$, $\eta=0.827$, $\Theta_i=1.08$, and $\mathrm{Re}_i=0$ (solid), 50 (dashed), and 100 (dotted): (a) $v_{\theta b}$, (b) v_{zb}, (c) Θ_b vs r.

the critical Taylor number $\overline{\mathrm{Ta}}_{i,\mathrm{crit}}$. [We note that critical values are represented by the solid curves in Figs. 3(a)–3(d), 5(a)–5(d), 7(a)–7(d), and 9(a)–9(d) of Sec. IV.]

To ensure that critical values are fully resolved, we checked convergence for a range of Θ_i at each Re_i, κ, and η combination considered in this work. We note that there is a strong dependence of the eigenfunction complexity on Re_i and the azimuthal wave number m, thus the number of collocation points needed to resolve the critical condition for a given Θ_i increases significantly with increasing Re_i and m. This strong dependence on azimuthal wave number was also found (but not elucidated) in the zero axial flow case[28] for nonaxisymmetric disturbances. We believe that the strong dependence of the critical conditions on both the axial flow

and azimuthal wave number is due to the development of a strong internal thermal layer which is driven by the high Peclét number nature of the fluid being considered in this work (where the Peclét number is defined as $\mathrm{Pe}_i=\mathrm{Pr}_i\mathrm{Ta}_i$). Because the number of collocation points needed to fully resolve the internal layer is large, we have also solved the linear stability problem by solving a two point boundary value problem (using the program SUPPORT) whose results are used to check solutions in parts of parameter space for which the spectral method approach requires significant spatial resolution. Comparison between the two methods is good, but limited due to the fact that the boundary value problem approach uses Newton iteration to find critical eigenvalues and the domain of convergence is very small. Because of this, we have implemented spectral domain decomposition in the spectral code. For this method, one matches the velocity and temperature first derivatives and the pressure at the element intersections. For a single element the resulting matrix eigenvalue problem is dense, whereas for multiple elements the global matrix eigenvalue system is sparse. For this reason, we implement the sparse eigenvalue solver ARPACK which finds only a specified number of eigenvalues clustered around a selected point (e.g., $\sigma=0$). In this work we keep the number of collocation points used per element fixed at $N_p^s=16$, and vary the number of elements (M) used depending on where we are in parameter space. Thus, we use enough elements to match the number of significant digits given by other authors when comparing to previous results, and enough to ensure graphical independence (i.e., the amount by which critical values are changing is less than what one would likely be able to see in a figure) of critical values when results are shown only graphically. For the results shown here, the maximum number of elements used was 10 (used for $\Theta_i=1.08$), whereas the number of elements used for most of the calculations was 7.

To validate the code, we compared our results to previous computational results for the stability of circular Couette flow with viscous heating. To the best of our knowledge, results are only available for the small-gap case, $\kappa\geqslant 0$, and zero axial flow (i.e., $\mathrm{Re}_i=0$). The most recent computational work is the narrow-gap results of Refs. 28 and 29. With regard to the fixed outer cylinder (i.e., $\kappa=0$) work of Al-Mubaiyedh *et al.*[28] we compare to results given in their Table 2 (we note that this is the only tabulated data given in their article) for $\Delta T=T_o-T_i=0$ K, $\eta=0.827$, and $m=0$. For this comparison, we use the fluid property data given in their Table 1, and take k to be constant and $\epsilon_2=\epsilon_3=0$. We have made these assumptions based on their governing equations and discussion. For $\Theta_i=1.03$ (i.e., $T_i=305.15$ K) and $m=0$, our computed values are $\dot{\gamma}=76.59\ \mathrm{s}^{-1}$, $\bar{a}=2.80$, $\bar{c}=0$, $\overline{\mathrm{Ta}_i}=34.52$, $\overline{\mathrm{Pr}_i}=4.111\times 10^3$, and $\overline{\mathrm{Na}_i}=0.1367$, whereas for $\Theta_i=1.06$ (i.e., $T_i=316.15$ K) our computed values are $\dot{\gamma}=68.97\ \mathrm{s}^{-1}$, $\bar{a}=2.91$, $\bar{c}=0$, $\overline{\mathrm{Ta}_i}=66.88$, $\overline{\mathrm{Pr}_i}=1.911\times 10^3$, and $\overline{\mathrm{Na}_i}=0.048\,31$. The magnitude of the maximum difference in $\overline{\mathrm{Ta}_i}$ is approximately 0.05%, whereas the magnitude of the maximum difference in $\bar{a}$ is approximately 1.4%. On the other hand, the magnitude of the differences between our computed $\dot{\gamma}$ and theirs are approximately 1.3% and 1.9% for $\Theta_i=1.03$ and 1.06, respectively. This would seem to suggest that our results and theirs are in good agreement, but we note that our results are very much in disagreement at high Θ_i (e.g., for $\overline{\mathrm{Na}_i}=0.1$ the magnitude of the difference in $\overline{\mathrm{Ta}_i}$ is approximately 14%, 7%, and 24% for $m=0$, 1, and 2, respectively, where we have read results from their Fig. 1). In the limit $T_i\rightarrow\infty$ ($\overline{\mathrm{Na}_i}\rightarrow 0$), Al-Mubaiyedh *et al.*[28] recover the isothermal constant property values of 101.29, 102.45, and 106.13 for $\overline{\mathrm{Ta}_i}$ (see Ref. 28, p. 117) for $m=0$, 1, and 2, respectively. This does not seem to be the correct asymptotic behavior for system (1), and we note that in the limit $T_i\rightarrow\infty$ one should recover the inviscid values, not the isothermal constant property results shown in their Figs. 1(a) and 1(b) for small $\overline{\mathrm{Na}_i}$ (see Refs. 6 and 8 for a detailed discussion of the isothermal constant property results). We believe that the problem arises from the fact that they seem to take $T_i=T_r$ in their work. We note that in the related $\kappa\neq 0$ work (Ref. 29, p. 3310), the authors indicate that this is in fact what has been done. This assumption would be consistent with their results for large T_i, because if one does set $T_i=T_r$ and takes $\epsilon_1\rightarrow 0$, the isothermal constant property results are recovered. Thus, we have recomputed the stability boundaries for $\mathrm{Re}_i=0$ in Sec. IV to show the correct behavior for large T_i. We note that the experimental results of White and Muller[25,32] are for the case of no axial flow (i.e., $\mathrm{Re}_i=0$), and point out that we know of no experimental results in which axial flow affects have been included.

IV. RESULTS

We report linear stability boundaries in the Θ_i-$\overline{\mathrm{Ta}_i}$ plane for $\mathrm{Re}_i=0$ and in the Re_i-$\overline{\mathrm{Ta}_i}$ plane for nonzero axial flow and various values of Θ_i. In this work, we take ϵ_2 and ϵ_3 to be 0 (i.e., the density and constant pressure specific heat are independent of temperature), fix the outer cylinder ($\kappa=0$), and consider a range of T_i similar to that investigated experimentally (i.e., $10\ ^\circ\mathrm{C}\leqslant T_i\leqslant 50\ ^\circ\mathrm{C}$ or $0.95\leqslant\Theta_i\leqslant 1.08$) by White and Muller[25,32] and numerically by Al-Mubaiyedh *et al.*[28] for $\mathrm{Re}_i=0$. We consider azimuthal wave numbers in the range $-2\leqslant m\leqslant 2$ and axial flow in the range $0\leqslant\mathrm{Re}_i\leqslant 100$. (We note that in Figs. 3, 5, and 7 dotted curves represent neutral curve extrema for a given m, whereas the solid curves in Figs. 3, 5, 7, and 9 represent critical values over the range of m considered.) In this work, when we refer to stability boundaries we mean the solid curves, not the dotted curves. For all the plots shown here, points on curves have been connected using spline curve fits. Dotted, dashed, and solid neutral curves (see Figs. 4, 6, 8, 10, and 11) correspond to $m<0$, $m=0$, and $m>0$, respectively.

A. Zero axial flow ($\mathrm{Re}_i=0$)

The $\mathrm{Re}_i=0$ results of Ref. 28 have been reproduced to show what we believe to be the correct behavior for large Θ_i, and to gauge the overall effect of axial flow on the linear stability of circular Couette flow with viscous heating. We note that for $\mathrm{Re}_i=0$, it can be shown that $\overline{\mathrm{Ta}_i}$, $\bar{a}$, and $\overline{\mathrm{Na}_i}$ are invariant to changes in the sign of m, whereas the sign of the wave speed ($\bar{c}=\sigma_i/\bar{a}$) depends on the sign of m. This is due

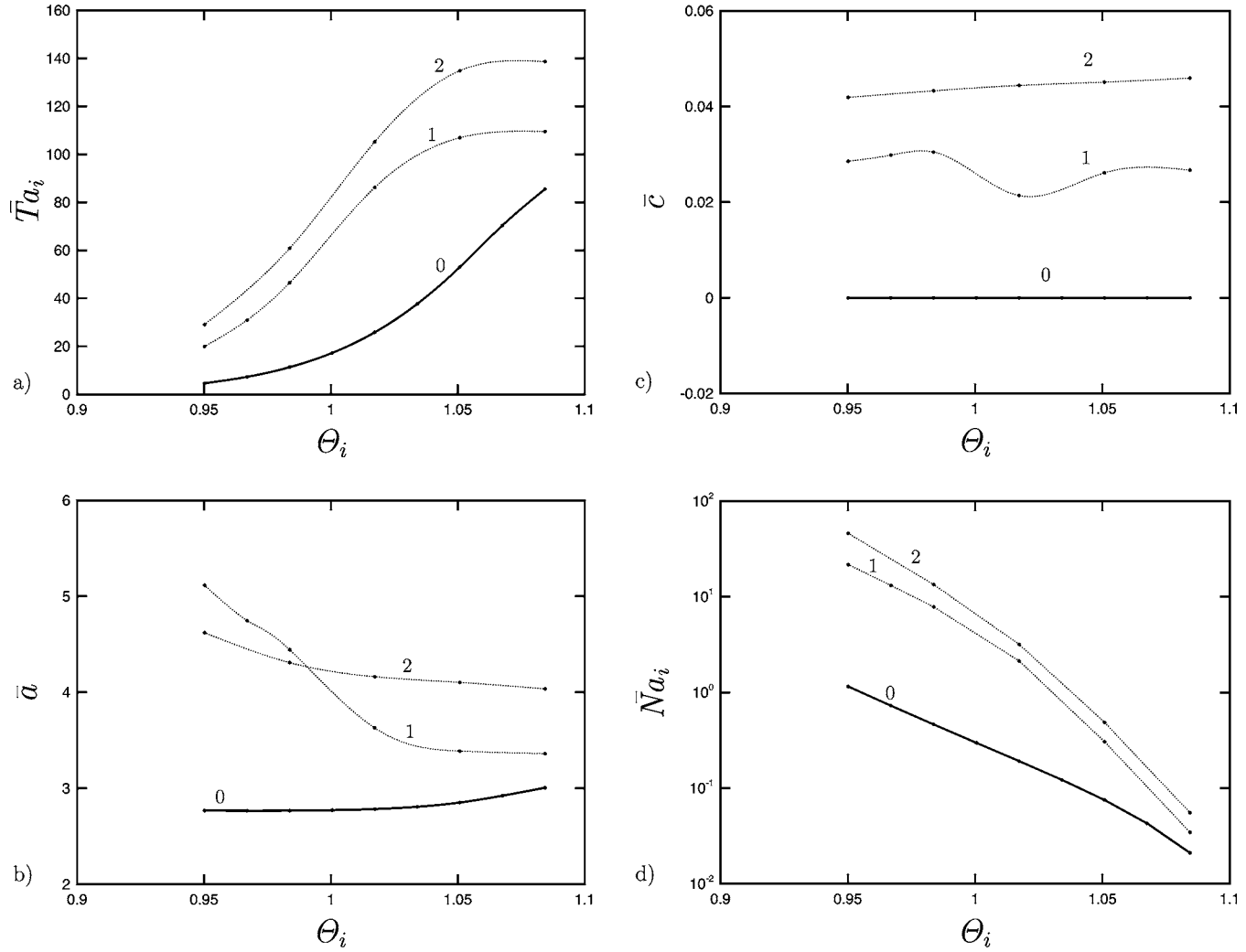

FIG. 3. For $\epsilon_2=\epsilon_3=0$, $\kappa=0$, $\eta=0.827$, and $\mathrm{Re}_i=0$: (a) $\overline{\mathrm{Ta}}_i$, (b) $\bar{a}$, (c) $\bar{c}$, (d) $\overline{\mathrm{Na}}_i$ vs Θ_i, where azimuthal wave numbers are shown and solid curves represent critical values.

to the fact that for $\mathrm{Re}_i=0$ critical eigenvalues are complex conjugates for $\pm m$. Thus, we show results for only positive values of the azimuthal wave number.

As shown in the stability boundaries of Fig. 3(a), viscous heating effects can be very strong, with results showing approximately an order of magnitude change in $\overline{\mathrm{Ta}}_i$ with wall temperature for axisymmetric ($m=0$) and nonaxisymmetric ($m\neq 0$) disturbances. We note that these results are in significant contrast to those of Ref. 28 at large Θ_i, where their results show that for azimuthal modes $m=1$ and $m=2$, $\overline{\mathrm{Ta}}_i$ asymptotes to nearly the same value. As stated in their article, these values of $\overline{\mathrm{Ta}}_i$ correspond to isothermal critical values for the constant property case, whereas as discussed in Sec. III, we believe that this is not the correct high-Θ_i behavior. As shown in Fig. 3(a), the solid curves represent the critical $\overline{\mathrm{Ta}}_i$ (i.e., $\overline{\mathrm{Ta}}_{i,\mathrm{crit}}$) as a function of Θ_i, and as can be seen, the critical disturbance is axisymmetric (i.e., $m_{\mathrm{crit}}=0$) over the entire range of Θ_i considered. Even though there are differences between the current results and those of Ref. 28 the critical $\mathrm{Re}_i=0$ disturbance is found to be axisymmetric over the entire temperature range considered in both works. Results suggest that in the limit of $\mathrm{Pe}_i\rightarrow\infty$, the base state is unstable for all $\overline{\mathrm{Ta}}_i$. This fact was suggested by results in which we expanded the velocity, pressure, and temperature in powers of $1/\mathrm{Pe}_i$ and considered the stability to zeroth order. As can be seen in Fig. 3(a), this is consistent with current results (and previous results), whereas Θ_i gets small Pe_i gets large and the critical $\overline{\mathrm{Ta}}_i$ seems to be going to 0.

Figure 4 shows neutral curves (i.e., a vs Ta_i) for $m=0$, 1, and 2 for values of Θ_i spanning the range considered here [i.e., see Fig. 4(a) for $\Theta_i=0.95$, Fig. 4(b) for $\Theta_i=1.02$, and Fig. 4(c) for $\Theta_i=1.08$]. Results show that neutral curves are all primary neutral curves (i.e., a curve defined by having a vertical asymptote at $a=0$, and apparently existing as $a\rightarrow\infty$) and that we have found no closed disconnected neutral curves (seen in cases for which the stability boundary is multivalued) such as found for the isothermal constant property case[6] for smaller η and at higher values of Θ_i in the current work [see Fig. 6(c)]. The discontinuities in the neutral curves of Fig. 4(a) correspond to mode changes, that is an eigenvalue that at lower values of Ta_i crossed into the RHP after the critical eigenvalue now crosses first; thus becoming the critical eigenvalue. Also, we see that the $m=2$ neutral curve is slightly bimodal [see Fig. 4(a)]. We also note that in Fig.

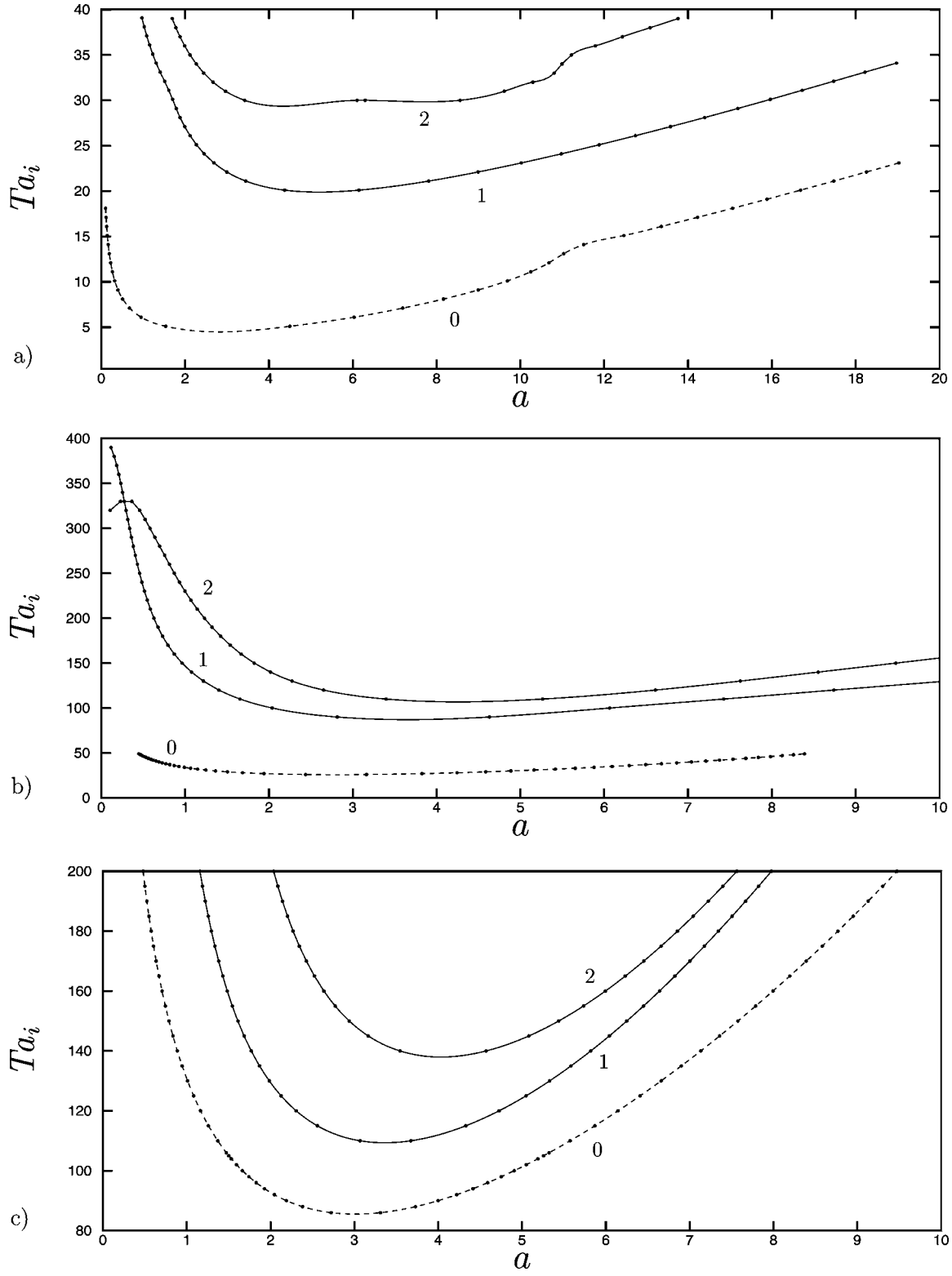

FIG. 4. Neutral curves for $\epsilon_2=\epsilon_3=0$, $\kappa=0$, $\eta=0.827$, and $\mathrm{Re}_i=0$: (a) $\Theta_i=0.95$, (b) $\Theta_i=1.02$, (c) $\Theta_i=1.08$, where values of the azimuthal wave number are shown.

4(b) for $\Theta_i=1.02$, the $m=0$ neutral curve is only a weak function of the axial wave number. This fact makes determination of the value of a at which Ta_i assumes its minimum much more difficult.

As shown in Fig. 3(b), the character of $\bar{a}$ greatly depends on whether or not the disturbance is axisymmetric. As shown by the solid curve, the critical disturbance is axisymmetric and $\bar{a}_{\mathrm{crit}}$ increases only slightly as Θ_i increases from 0.95 to 1.08. As shown in Fig. 3(c), the minimum disturbance is steady for $m=0$, and unsteady for nonzero m. In contrast to the results for $\overline{\mathrm{Ta}}_i$ and $\bar{a}$ [Figs. 3(a) and 3(b)], $\bar{c}$ is not invariant with respect to the sign of m, and takes on both positive

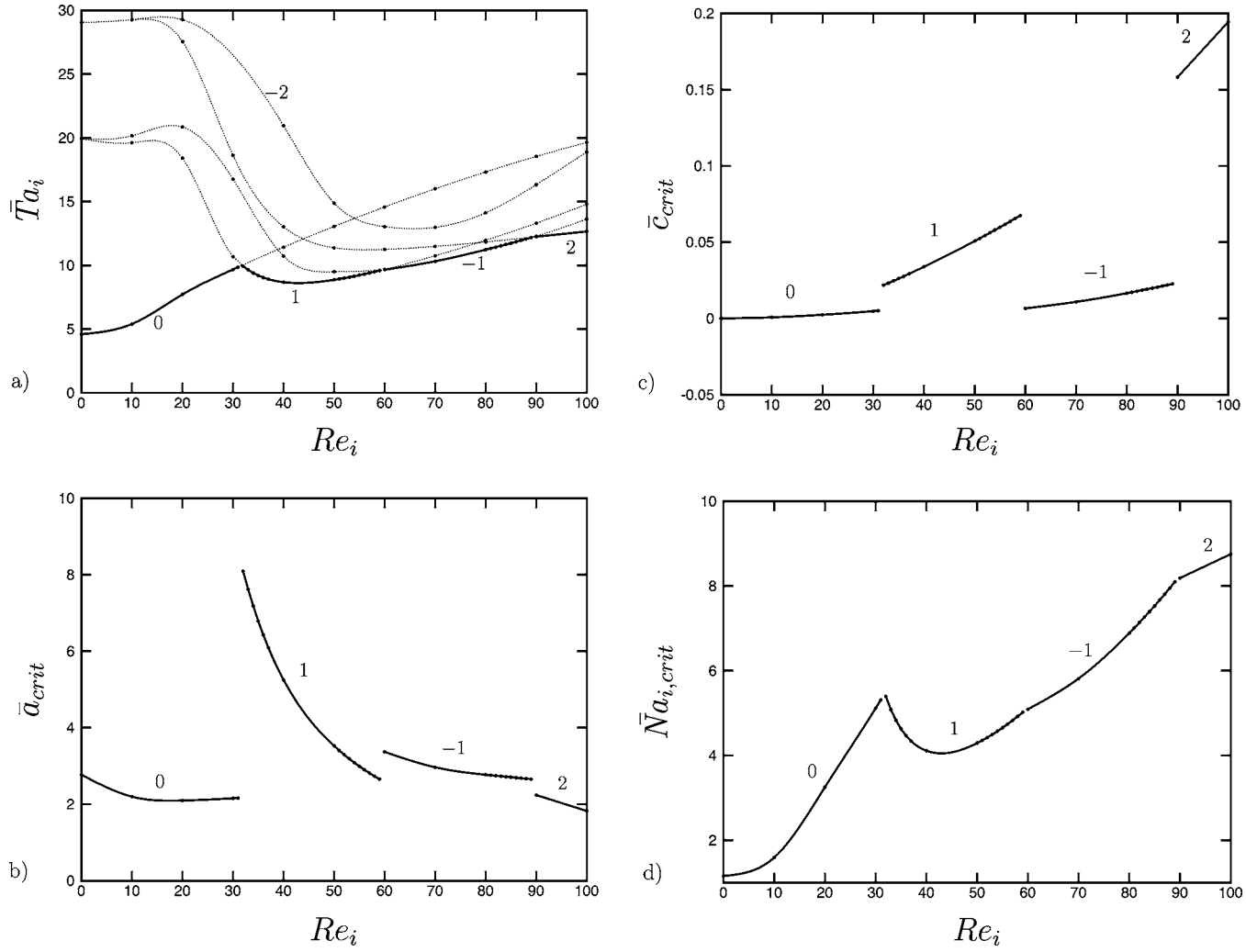

FIG. 5. For $\epsilon_2=\epsilon_3=0$, $\kappa=0$, $\eta=0.827$, and $\Theta_i=0.95$: (a) $\overline{\mathrm{Ta}}_i$, (b) critical $\bar{a}$, (c) critical $\bar{c}$, (d) critical $\overline{\mathrm{Na}}_i$ vs Re_i, where azimuthal wave numbers are shown and solid curves represent critical values.

$(m>0)$ and negative $(m<0)$ values. As shown by the solid curve, $\bar{c}_{\mathrm{crit}}$ is 0 (i.e., $\sigma_i=0$) over the entire range of Θ_i considered. We note that critical values of $\overline{\mathrm{Na}}_i$ are denoted by the solid curve in Fig. 3(d), and that $\overline{\mathrm{Na}}_{i,\mathrm{crit}}$ monotonically decreases with increasing Θ_i. As shown in Fig. 3(d), $\overline{\mathrm{Na}}_i$ (representing the maximum fractional change in the viscosity under the action of viscous heating) changes by almost two orders of magnitude for $m=0$ over the temperature range considered in the present work. For each Θ_i considered, $\overline{\mathrm{Na}}_i$ increases with increasing m, and the difference between axisymmetric and nonaxisymmetric values decrease as one goes from low to high wall temperatures.

B. Nonzero axial flow ($\mathrm{Re}_i\neq 0$)

In this section, we discuss linear stability results for nonzero Re_i $(0\leqslant \mathrm{Re}_i\leqslant 100)$ and $\Theta_i=0.95$, 1.02, and 1.08 (Figs. 5, 7, and 9), and show results for azimuthal wave numbers in the range $-2\leqslant m\leqslant 2$. We note that for nonzero axial flow $(\mathrm{Re}_i\neq 0)$, values of $\overline{\mathrm{Ta}}_i$, $\bar{a}$, and $\overline{\mathrm{Na}}_i$ are no longer invariant with respect to the sign of m as they were for $\mathrm{Re}_i=0$.

1. $\Theta_i=0.95$

Figure 5(a) shows linear stability results (dotted curves) versus Re_i for $\Theta_i=0.95$ and $m=0$, ±1, and ±2. As can be seen in Fig. 5(a), $\overline{\mathrm{Ta}}_i$ varies significantly with Re_i and m. We note that at large Re_i, the values of $\overline{\mathrm{Ta}}_i$ for $m=\pm2$ depart significantly. This is in contrast to the behavior seen for $m=\pm1$, where $\overline{\mathrm{Ta}}_i$ for both values of m remain close as Re_i approaches 100. For the range of azimuthal wave numbers considered here, the solid lines in Fig. 5(a) represent the critical $\overline{\mathrm{Ta}}_i$ as a function of Re_i. The critical disturbance is axisymmetric $(m=0)$ for Re_i less than approximately 30, whereas the critical azimuthal wave number is $m=1$ for $30<\mathrm{Re}_i\leqslant 60$, $m=-1$ for $60<\mathrm{Re}_i\leqslant 88$, and $m=2$ for $\mathrm{Re}_i>88$. As Re_i increases from 0, $\overline{\mathrm{Ta}}_{i,\mathrm{crit}}$ increases by approximately a factor of 2 until reaching the point where m_{crit} discontinuously changes from 0 to 1 (a local maximum). As Re_i increases beyond this point, $\overline{\mathrm{Ta}}_{i,\mathrm{crit}}$ initially decreases on the $m_{\mathrm{crit}}=1$ portion of the stability boundary until reaching a local minimum. Then as Re_i is increased beyond this local minimum, $\mathrm{Ta}_{i,\mathrm{crit}}$ increases monotonically for each constant-m_{crit} portion

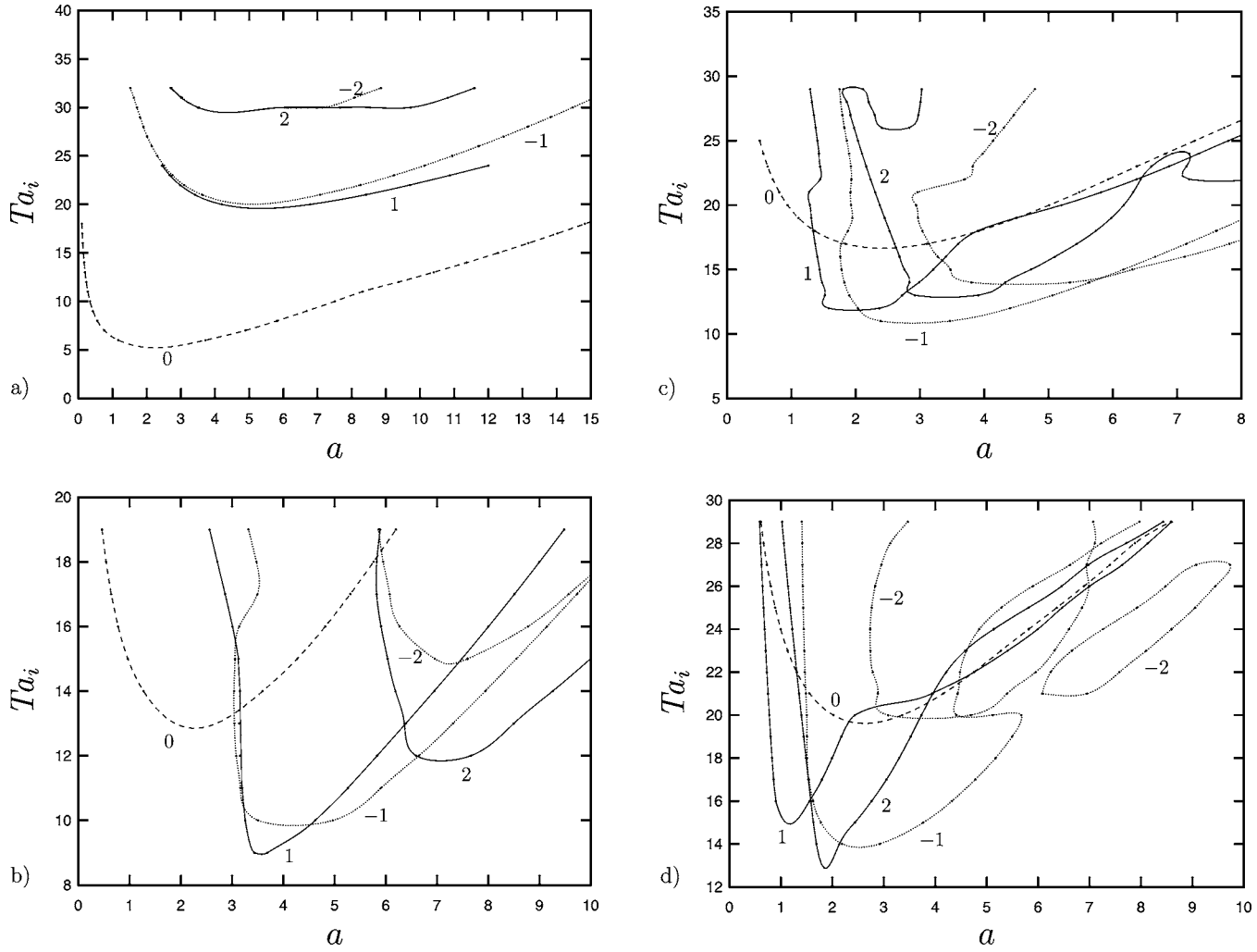

FIG. 6. Neutral curves for $\epsilon_2=\epsilon_3=0$, $\kappa=0$, $\eta=0.827$, and $\Theta_i=0.95$: (a) $\mathrm{Re}_i=10$, (b) $\mathrm{Re}_i=50$, (c) $\mathrm{Re}_i=75$, (d) $\mathrm{Re}_i=100$, where values of the azimuthal wave number are shown.

of the stability boundary. We note that $\overline{\mathrm{Ta}}_{i,\mathrm{crit}}$ has increased by approximately 176% at $\mathrm{Re}_i=100$ compared to its $\mathrm{Re}_i=0$ value.

Figure 6 shows neutral curves for $m=0$, ±1, and ±2 for values of Re_i spanning the range considered here [i.e., see Fig. 6(a) for Re=10, Fig. 6(b) for Re=50, Fig. 6(c) for Re =75, and Fig. 6(d) for Re=100]. We note that neutral curves are all primary neutral curves, except for $\mathrm{Re}_i=100$ where we have found both primary and closed disconnected neutral curves for $m=-2$. As one increases axial flow, the neutral curves become increasingly more complex. As was also the case for $\mathrm{Re}_i=0$, we see that for some of the nonaxisymmetric neutral curves the minimum is only a very slight function of the axial wave number (i.e., the neutral curve nose is flat), which can cause numerical difficulties in determining the critical axial wave number. On the other hand, for some values of m_{crit} (i.e., $m=0$ for $\mathrm{Re}_i=10$, $m=1$ for $\mathrm{Re}_i=50$, and $m=2$ for $\mathrm{Re}_i=100$) the minimum in the neutral curve is very easily found because the nose of the neutral curve is fairly sharp.

As shown in Fig. 5(b) by the solid curves, $\bar{a}_{\mathrm{crit}}$ varies by approximately a factor of 4 over the entire range of Re_i considered here, with $\bar{a}_{\mathrm{crit}}$ assuming its maximum for $m_{\mathrm{crit}}=1$ and intermediate values of Re_i. As can be seen in Fig. 5(b), most of the variation in $\bar{a}_{\mathrm{crit}}$ happens when $m_{\mathrm{crit}}=1$. As shown in Fig. 5(c) by the solid curves, $\bar{c}_{\mathrm{crit}}$ varies significantly over the range of Re_i considered in this work, and is positive over the entire range of nonzero Re_i investigated. As also can be seen in Fig. 5(c), $\bar{c}_{\mathrm{crit}}$ is a very strong function of the azimuthal wave number. As shown in Fig. 5(d) by the solid curves, results for $\overline{\mathrm{Na}}_i$ are qualitatively similar to those of $\overline{\mathrm{Ta}}_i$, and we note that there is an overall increase in $\overline{\mathrm{Na}}_{i,\mathrm{crit}}$ as Re_i increases from 0 to 100. This is consistent with the fact that at high Re_i viscous heating becomes more important because of the added effects of axial shear.

2. $\Theta_i=1.02$

Figure 7(a) shows linear stability results (dotted curves) versus Re_i for $\Theta_i=1.02$ and $m=0$, ±1, and ±2. As can be seen in Fig. 7(a), $\overline{\mathrm{Ta}}_i$ varies significantly with Re_i and m, even more than for $\Theta_i=0.95$. The critical disturbance is axisymmetric ($m=0$) for Re_i less than approximately 15, whereas the critical azimuthal wave number is $m=1$ for $17<\mathrm{Re}_i \leqslant 53$, and again $m=0$ (i.e., axisymmetric) for $\mathrm{Re}_i>53$. As was the case for $\Theta_i=0.95$, $\overline{\mathrm{Ta}}_{i,\mathrm{crit}}$ is nonmonotonic over the

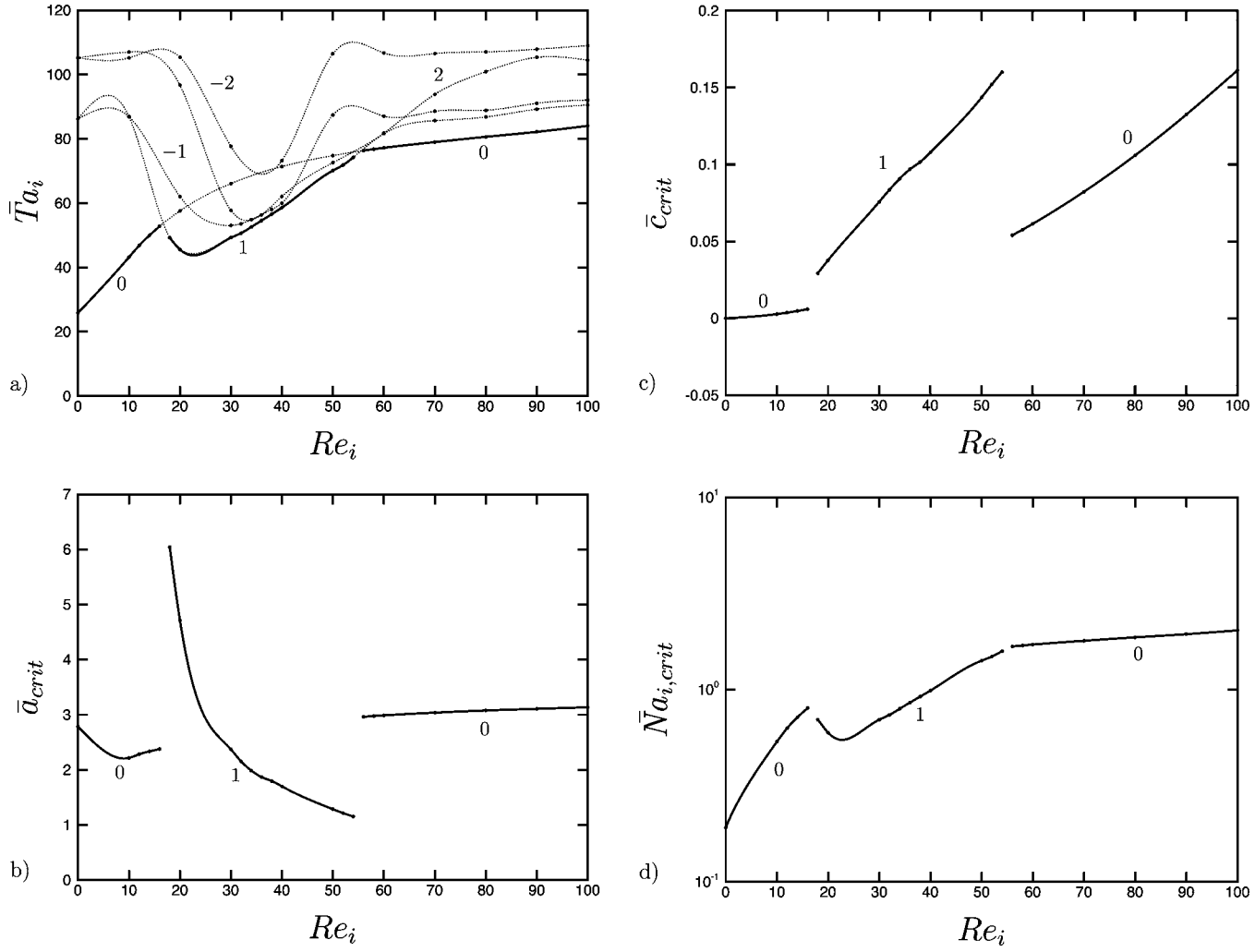

FIG. 7. For $\epsilon_2=\epsilon_3=0$, $\kappa=0$, $\eta=0.827$, and $\Theta_i=1.02$: (a) $\overline{\mathrm{Ta}}_i$, (b) critical $\bar{a}$, (c) critical $\bar{c}$, (d) critical $\overline{\mathrm{Na}}_i$ vs Re_i, where azimuthal wave numbers are shown and solid curves represent critical values.

entire range of Re_i considered, and assumes a local minimum at an Re_i of approximately 22, which is less than the corresponding $\Theta_i=0.95$ value of approximately 40. The behavior seen in Fig. 7(a), namely that the critical disturbance becomes axisymmetric again at higher Re_i, is a new feature of spiral Poiseuille flow seen for the first time here and is assumed to be due to viscous heating effects. We note that $\overline{\mathrm{Ta}}_{i,\mathrm{crit}}$ has increased by approximately 200% at $\mathrm{Re}_i=100$ when compared to its $\mathrm{Re}_i=0$ value.

Figure 8 shows neutral curves for $m=0$, ±1, and ±2 for values of Re_i spanning the range considered here [i.e., see Fig. 8(a) for $\mathrm{Re}_i=10$, Fig. 8(b) for $\mathrm{Re}_i=50$, and Fig. 8(c) for $\mathrm{Re}_i=100$]. As can be seen from Fig. 8(a), for $\mathrm{Re}_i=10$ the neutral curves for $m=\pm1$ and $m=\pm2$ coincide over a wide range of a which includes the minimum. We note that in contrast to the results for $\Theta_i=0.95$, for $\Theta_i=1.02$ we have found only primary neutral curves, and all neutral curves seem to have only one minimum except for the $m=0$ and $m=2$ neutral curves [Figs. 8(a) and 8(c)] for $\mathrm{Re}=10$ and 100, respectively, which are bimodal and have a local minimum at low a. Also, neutral curves for $\Theta_i=1.02$ are much less complex in nature than those found at intermediate- and high-Re values for $\Theta_i=0.95$, which is consistent with the fact that as Θ_i increases the coupling between the disturbance momentum and energy equations (due to viscous heating effects) is becoming less important.

As shown in Fig. 7(b) by the solid curves, $\bar{a}_{\mathrm{crit}}$ changes only slightly over the range of Re_i considered here (approximately 10% at low Re_i) for $m=0$, whereas for $m=1$ $\bar{a}_{\mathrm{crit}}$ varies by approximately 83% over the range of Re_i for which $m_{\mathrm{crit}}=1$. For $m_{\mathrm{crit}}=0$ and high Re_i, $\bar{a}_{\mathrm{crit}}$ increases monotonically to its value at $\mathrm{Re}_i=100$, a value similar to its $\mathrm{Re}_i=0$ value. We note that the overall behavior is similar to that for $\Theta_i=0.95$, with the most variation in $\bar{a}_{\mathrm{crit}}$ seen for $m_{\mathrm{crit}}=1$. As shown in Fig. 7(c) by the solid curves, $\bar{c}_{\mathrm{crit}}$ varies significantly over the range of Re_i considered in this work, and is positive over the entire range of nonzero Re_i investigated, which is similar to what we saw for $\Theta_i=0.95$. As shown in Fig. 7(d) by the solid curves, results for $\overline{\mathrm{Na}}_{i,\mathrm{crit}}$ are qualitatively similar to those of $\overline{\mathrm{Ta}}_{i,\mathrm{crit}}$, and we note that there is an overall increase in $\overline{\mathrm{Na}}_{i,\mathrm{crit}}$ as Re_i increases from 0 to 100, with a pronounced local minimum at an Re_i of approximately 22 for $m_{\mathrm{crit}}=1$. This overall increase in $\overline{\mathrm{Na}}_{i,\mathrm{crit}}$ was also found for $\Theta=0.95$.

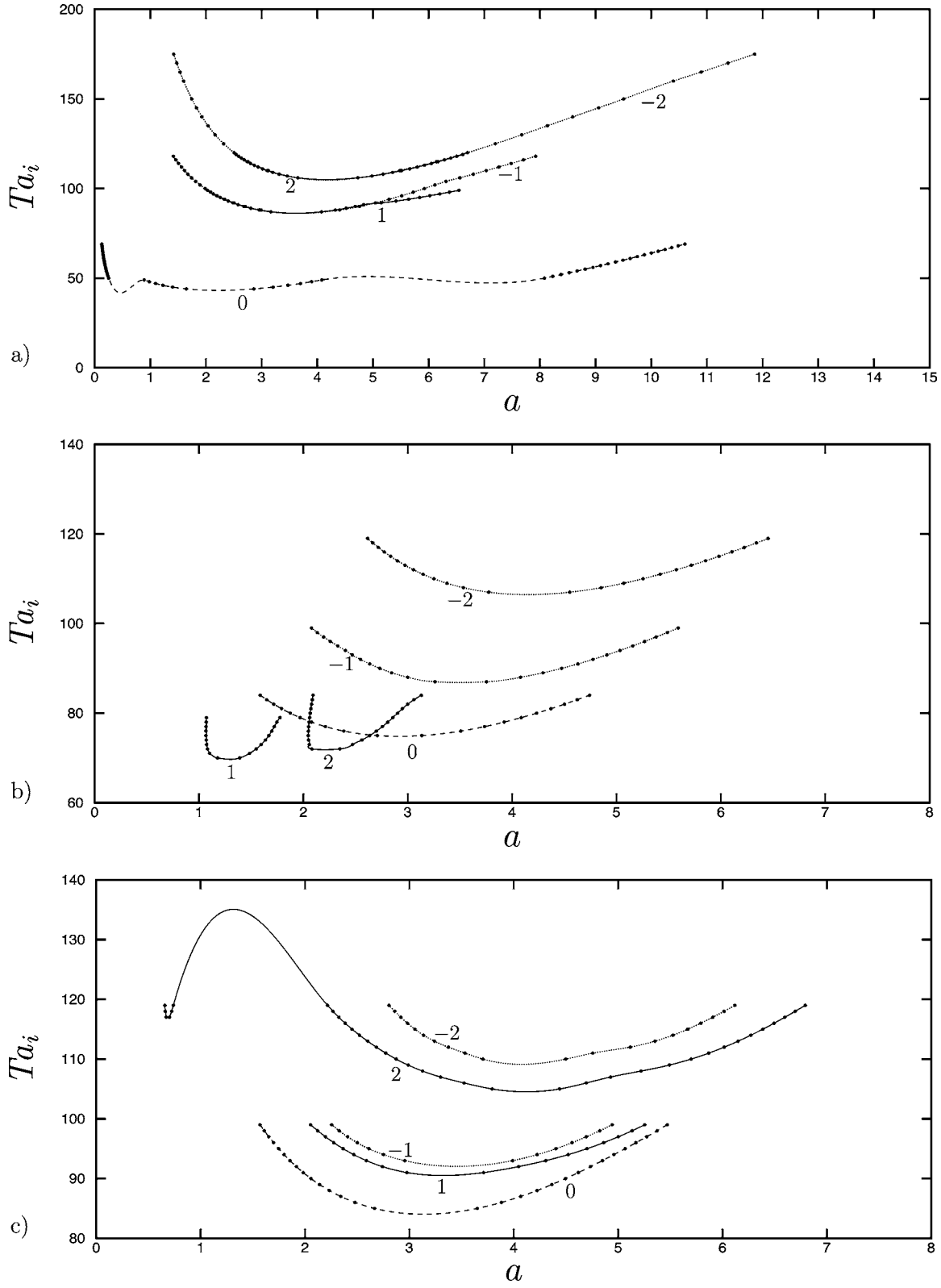

FIG. 8. Neutral curves for $\epsilon_2=\epsilon_3=0$, $\kappa=0$, $\eta=0.827$, and $\Theta_i=1.02$: (a) $\mathrm{Re}_i=10$, (b) $\mathrm{Re}_i=50$, (c) $\mathrm{Re}_i=100$, where values of the azimuthal wave number are shown.

3. $\Theta_i=1.08$

For $\Theta_i=1.08$, we have decided to show only critical values (solid curves) versus Re_i instead of following the format used in the previous two sections for $\Theta_i=0.95$ and 1.02. This decision was made because the values of $\overline{\mathrm{Ta}_i}$, for the values of m considered in this work, are so close in magnitude that the previous format is infeasible [cf. Figs. 10(c) and 11]. This is in contrast to the behavior seen for $\Theta_i=0.95$ and 1.02, where $\overline{\mathrm{Ta}_i}$ was a very strong function of the azimuthal wave number.

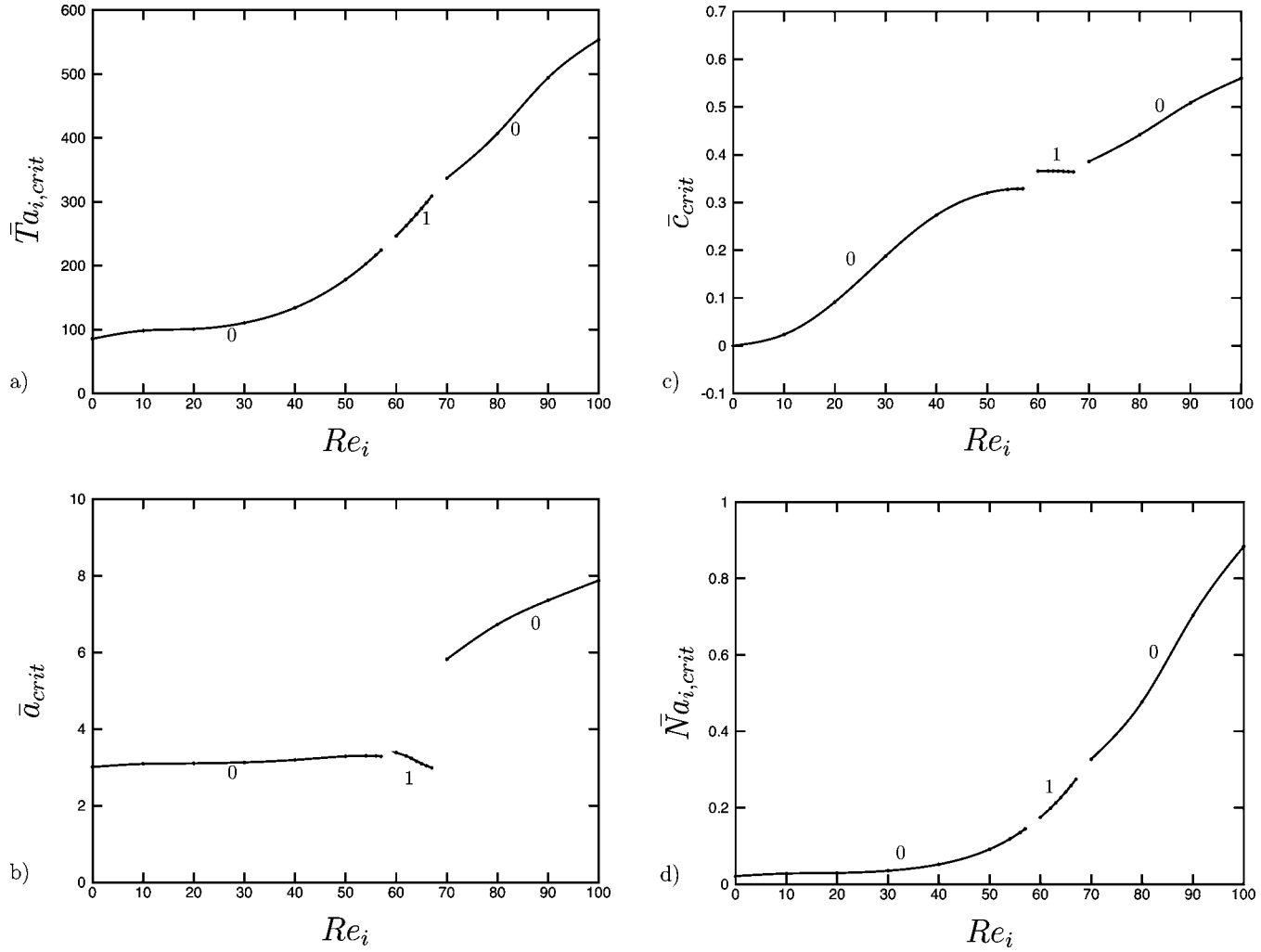

FIG. 9. For $\epsilon_2=\epsilon_3=0$, $\kappa=0$, $\eta=0.827$, and $\Theta_i=1.08$: (a) critical $\overline{\mathrm{Ta}}_i$, (b) critical $\bar{a}$, (c) critical $\bar{c}$, (d) critical $\overline{\mathrm{Na}}_i$ vs Re_i, where critical azimuthal wave numbers are shown.

As can be seen in Fig. 9(a), $\overline{\mathrm{Ta}}_{i,\mathrm{crit}}$ varies significantly with Re_i, and as Re_i increases from 0 $\overline{\mathrm{Ta}}_{i,\mathrm{crit}}$ ($m_{\mathrm{crit}}=0$ at $\mathrm{Re}_i=0$) increases until reaching its maximum at $\mathrm{Re}_i=100$. As shown in Figs. 10(a) and 10(b), neutral curves for $m=0$, ±1, and ±2 are all primary neutral curves. Values of Ta_i for $m=\pm1$ and $m=\pm2$ lie very close to each other for $\mathrm{Re}_i=10$, whereas for $\mathrm{Re}_i=50$ these neutral curves are significantly more spaced out. In contrast to results at low and intermediate Re_i, for Re_i greater than approximately 50 things start to become much more complicated. As can be seen in Fig. 10(c) for $\mathrm{Re}_i=70$, neutral curve complexity has increased and neutral curves are now slightly bimodal in nature (i.e., exhibit multiple extrema). [We note that when a neutral curve is bimodal there exists the possibility of a discontinuous change in critical axial wave number (i.e., $\bar{a}_{\mathrm{crit}}$) without a change in critical azimuthal wave number, i.e., m_{crit}.] This behavior is in contrast to the behavior seen for $\Theta_i=0.95$ and 1.02, where all critical neutral curves were primarily unimodal in nature, and any discontinuous change in $\bar{a}_{\mathrm{crit}}$ was a direct consequence of a change in m_{crit}. As shown in Figs. 11(a)–11(c), this bimodal behavior of the neutral curves becomes much more pronounced as Re_i increases beyond 70, with the global minimum for each m being at low values of a, whereas at high values of a there exists a second local minimum corresponding to a small wavelength instability. Results for $\mathrm{Re}\leqslant50$ are similar to those found for $\Theta_i=0.95$ and 1.02, where minimum values of Ta_i (i.e., $\overline{\mathrm{Ta}}_i$) are found at small a, whereas in contrast to the results at lower wall temperatures, for $\mathrm{Re}_i>70$ a local minimum is found at much larger values of a. We also note that only primary neutral curves have been found for $\Theta_i=1.08$. As shown in Fig. 9(a), the critical disturbance is axisymmetric ($m_{\mathrm{crit}}=0$) for $0\leqslant\mathrm{Re}_i<60$, whereas $m_{\mathrm{crit}}=1$ for $60\leqslant\mathrm{Re}_i<70$, and $m_{\mathrm{crit}}=0$ for $\mathrm{Re}_i\geqslant70$. As seen in Figs. 11(b) and 11(c) the minimum value of $\overline{\mathrm{Ta}}_{i,\mathrm{crit}}$ for $m=0$ and $m=1$ is very close, thus there seems to be a range of azimuthal wave numbers for which the critical Taylor number is for all practical purposes invariant with m, which was not the case for any of the previous values of Θ_i. As can be seen in Fig. 9(a), $\overline{\mathrm{Ta}}_{i,\mathrm{crit}}$ has increased by a factor of approximately 6.5 (i.e., a change of approximately 85%) at $\mathrm{Re}_i=100$ when compared to its $\mathrm{Re}_i=0$ value. Also, in contrast to the results for $\Theta_i=0.95$ and 1.02, where there were significant local extrema in the critical curves, here for a large portion of the stability boundary $\overline{\mathrm{Ta}}_{i,\mathrm{crit}}$ increases monotonically with increasing Re_i.

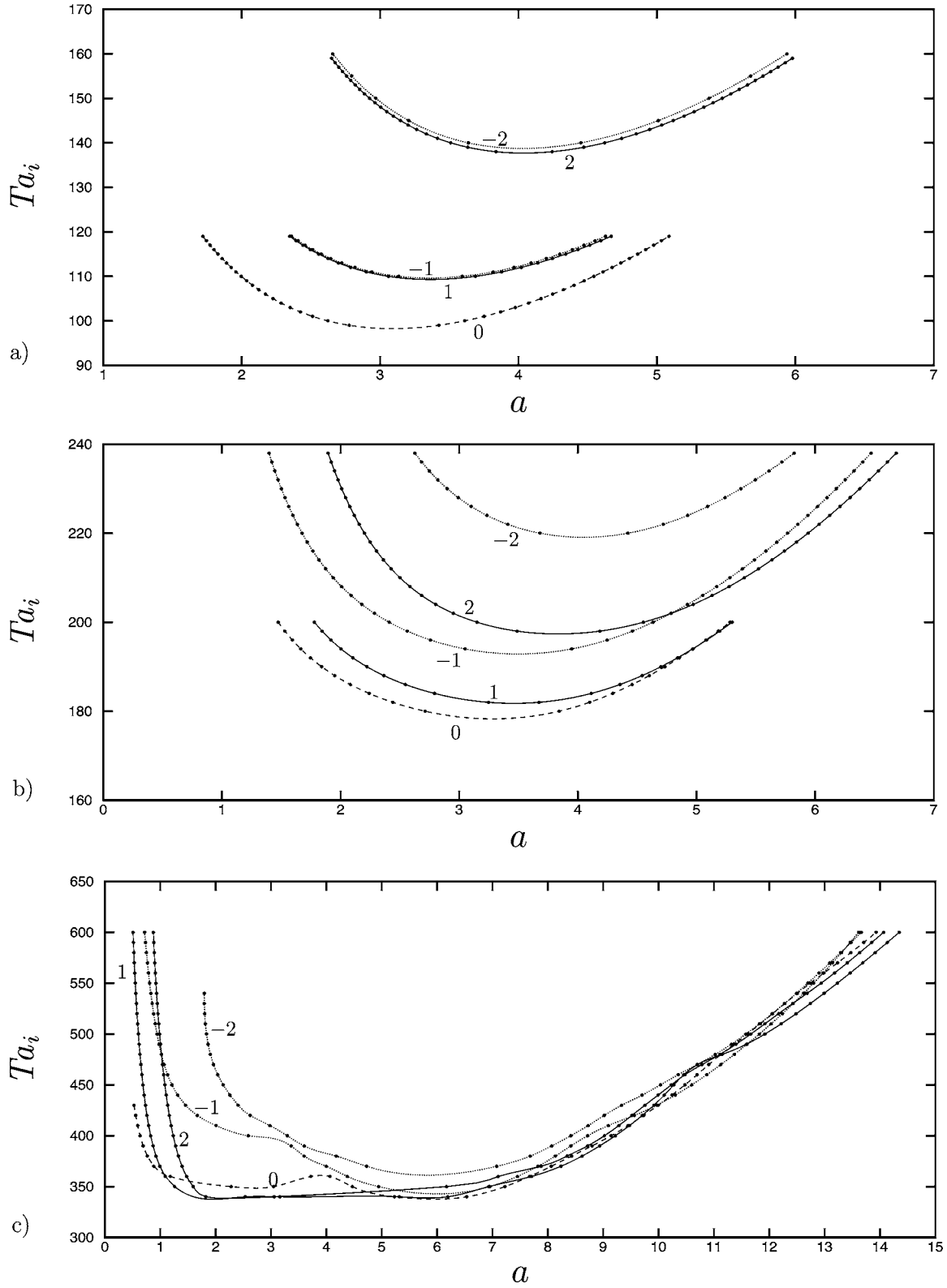

FIG. 10. Neutral curves for $\epsilon_2=\epsilon_3=0$, $\kappa=0$, $\eta=0.827$, and $\Theta_i=1.08$: (a) $\mathrm{Re}_i=10$, (b) $\mathrm{Re}_i=50$, (c) $\mathrm{Re}_i=70$, where values of the azimuthal wave number are shown.

As shown in Fig. 9(b) by the solid curves, $\bar{a}_{\mathrm{crit}}$ remains fairly unchanged as Re_i increases from 0 to approximately 60, where m_{crit} jumps from 0 to 1. As Re_i increases on the $m_{\mathrm{crit}}=1$ portion of the stability boundary, $\bar{a}_{\mathrm{crit}}$ decreases monotonically until m_{crit} jumps back to 0 at an Re_i of approximately 70. For the high-Re_i portion of the stability boundary ($m_{\mathrm{crit}}=0$), $\bar{a}_{\mathrm{crit}}$ increases monotonically until reaching its global maximum of approximately 8 at $\mathrm{Re}_i=100$. As shown in Fig. 9(c) by the solid curves, $\bar{c}_{\mathrm{crit}}$ is positive over the entire range of Re_i considered. On the $m_{\mathrm{crit}}=1$ portion of

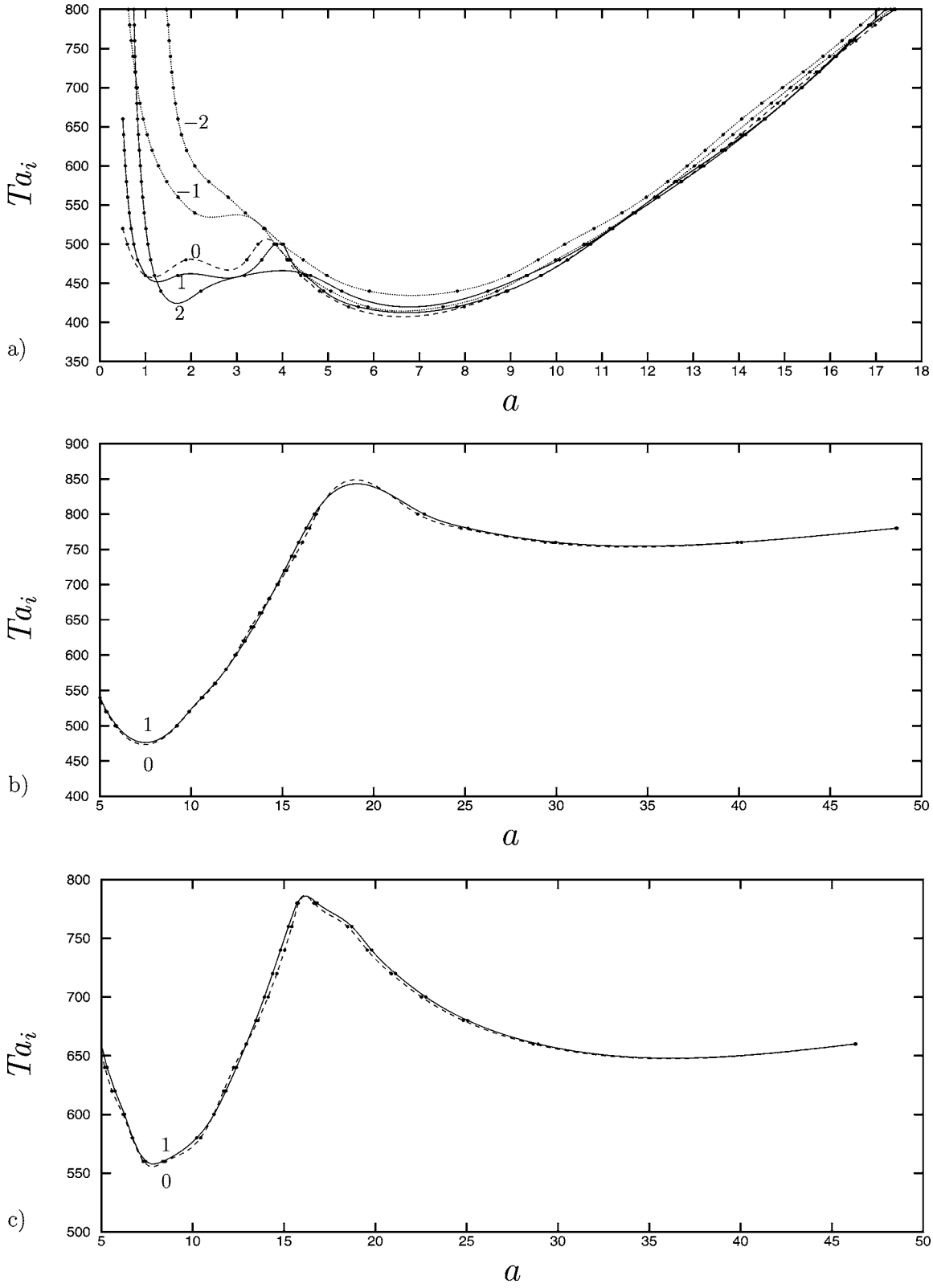

FIG. 11. Neutral curves for $\epsilon_2=\epsilon_3=0$, $\kappa=0$, $\eta=0.827$, and $\Theta_i=1.08$: (a) $\mathrm{Re}_i=80$, (b) $\mathrm{Re}_i=90$, (c) $\mathrm{Re}_i=100$, where values of the azimuthal wave number are shown.

the stability boundary, $\bar{c}_{\mathrm{crit}}$ varies very little. This is in contrast to the behavior seen on the other portions of the stability boundary, where $\bar{c}_{\mathrm{crit}}$ increases with increasing Re_i. As shown in Fig. 9(d), $\overline{\mathrm{Na}}_{i,\mathrm{crit}}$ increases monotonically with increasing Re_i for each constant-m_{crit} portion of the stability boundary, reaching its global maximum at $\mathrm{Re}_i=100$. This overall increase in $\overline{\mathrm{Na}}_{i,\mathrm{crit}}$ is consistent with the results at $\Theta_i=0.95$ and 1.02.

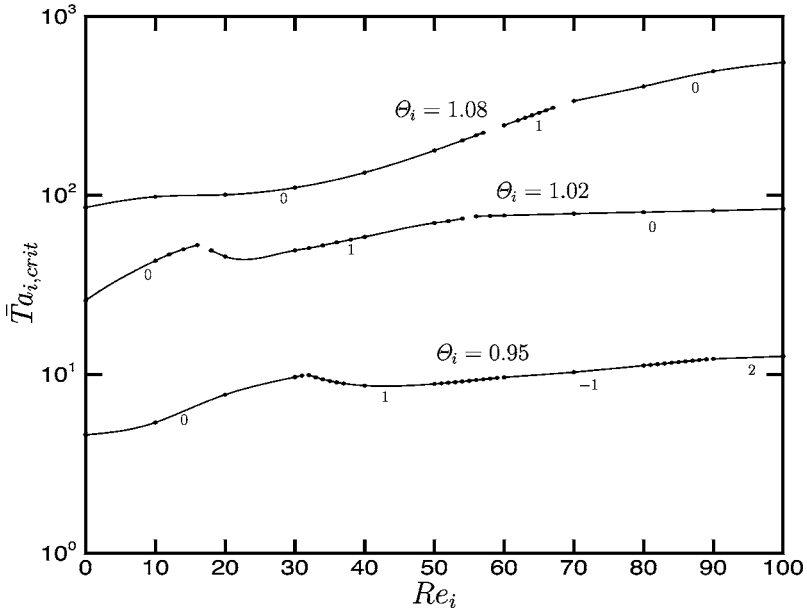

FIG. 12. Critical $\overline{\mathrm{Ta}}_i$ vs Re_i for $\epsilon_2=\epsilon_3=0$, $\kappa=0$, and $\eta=0.827$, where values of Θ_i and m_{crit} are shown.

V. DISCUSSION

A. Comparison of critical values for various wall temperatures

In this section, we discuss the differences between the critical values shown by the solid curves in Figs. 5, 7, and 9 for $\Theta_i=0.95$, 1.02, and 1.08, respectively.

As shown in Fig. 12, $\overline{\mathrm{Ta}}_{i,\mathrm{crit}}$ increases with increasing Θ_i for each value of Re_i considered. This would seem to be consistent with what one would expect as Θ_i becomes large, because the affect of the viscous terms in the disturbance equations is getting smaller due to the fact that f is getting smaller. Thus, one would expect that in the limit of $f\rightarrow 0$ that the base flow would be stable due to Rayleigh's inflection-point theorem (at least to axisymmetric disturbances). We also see that at low Re_i, the critical disturbance is axisymmetric for all wall temperatures considered, and that the range of Re_i for which this is true is a strong function of the wall temperature (i.e., Θ_i). We note that this range is largest for $\Theta_i=1.08$ and smallest for $\Theta_i=1.02$. Also, the difference between $\overline{\mathrm{Ta}}_{i,\mathrm{crit}}$ for $\Theta_i=0.95$ and 1.02 at $\mathrm{Re}_i=0$ is approximately the same as the difference between these two temperatures at $\mathrm{Re}_i=100$, whereas we see that the difference between $\overline{\mathrm{Ta}}_{i,\mathrm{crit}}$ for $\Theta_i=1.02$ and 1.08 has significantly increased at $\mathrm{Re}_i=100$ compared to the difference between these two temperatures at $\mathrm{Re}_i=0$. As shown in Fig. 12, the slope of the stability boundary at $\mathrm{Re}_i=100$ for $\Theta_i=0.95$ and 1.02 has begun to decrease, whereas for $\Theta_i=1.08$ we see that $\overline{\mathrm{Ta}}_{i,\mathrm{crit}}$ is still increasing at high Re_i. Overall, we see that for each wall temperature considered axial flow has a stabilizing affect on transition when compared to the $\mathrm{Re}_i=0$ case, and that at high Re_i and low wall temperature, $\overline{\mathrm{Ta}}_{i,\mathrm{crit}}$ seems to be approaching a plateau value. As can be seen by comparing Figs. 5(b), 7(b), and 9(b) for fixed Re_i, $\bar{a}_{\mathrm{crit}}$ varies significantly with temperature over most of the Reynolds number range considered, with the maximum occurring for low Θ_i and the minimum occurring for intermediate values of Θ_i, whereas the difference between values of $\bar{c}_{\mathrm{crit}}$ [see Figs. 5(c), 7(c), and 9(c)] for $\Theta_i=0.95$ and 1.02 varies very little over the range of Reynolds numbers considered, with the maximum difference occurring at high Re_i. On the other hand, for $\Theta_i=1.08$ we see that values of $\bar{c}_{\mathrm{crit}}$ differ significantly from those at lower Θ_i over most of the Reynolds number range considered.

B. Comparison to previous numerical and experimental results

In this section, we compare to the isothermal constant property results of Cotrell *et al.*[8] and to the $\mathrm{Re}_i=0$ experimental results of White and Muller.[25,32] We note that the current value of η lies between values of the radius ratio (i.e., $\eta=0.77$ and $\eta=0.95$) for which complete linear stability boundaries have been computed in Ref. 8. Thus, in order to facilitate a detailed comparison we have computed the isothermal constant property linear stability boundary for $\eta=0.827$, $\kappa=0$, and $0\leqslant \mathrm{Re}_i\leqslant 100$ (see Fig. 13).

To start with, we consider the comparison of the current results which include the effects of viscous heating to that of the isothermal constant property results shown in Fig. 13 and discussed in detail in Ref. 8 for values of η close to the present value. We note that isothermal constant property results shown in Fig. 13 use the current scaling, and that this scaling is different than used in Ref. 8 (e.g., a Re_i value of 100 corresponds to a Reynolds number of approximately 833 in Ref. 8 where we have assumed that properties (e.g., viscosity) in the isothermal constant property results of Ref. 8 are evaluated at the current reference temperature T_r). Results show that the base flow may be stabilized or destabilized (see Figs. 12 and 13) with respect to the isothermal constant property case depending on the value of the wall temperature and Reynolds number. For $\Theta_i=0.95$ the base flow becomes unstable at values of $\overline{\mathrm{Ta}}_{i,\mathrm{crit}}$ well below those of the isothermal constant property case, whereas for $\Theta_i=1.02$ the base flow becomes unstable at values of $\overline{\mathrm{Ta}}_{i,\mathrm{crit}}$ significantly closer to those of the isothermal constant prop-

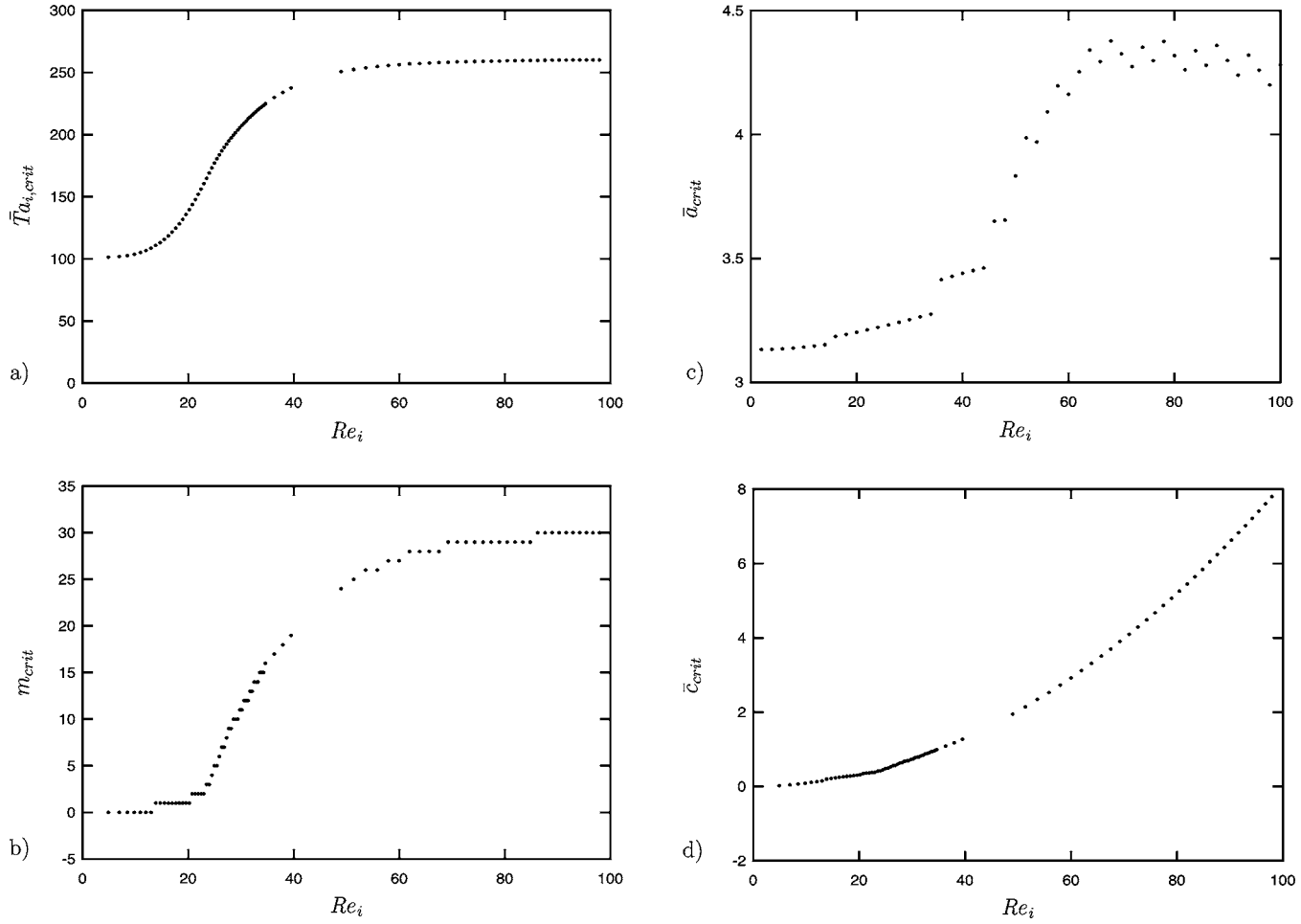

FIG. 13. Isothermal constant property results for $\eta=0.827$ and $\kappa=0$: (a) critical $\overline{\mathrm{Ta}}_i$, (b) critical m, (c) critical $\bar{a}$, (d) critical $\bar{c}$ vs Re_i.

erty case. As seen by comparing Figs. 12 and 13(a), for $\Theta_i=1.08$ the critical $\overline{\mathrm{Ta}}_i$ is very close to that of the isothermal constant property case for small Re_i, whereas at intermediate values of Re_i the current results show significant destabilization with respect to the constant property results, and conversely considerable stabilization at high Re_i. In contrast to the isothermal constant property results shown in Fig. 13, where m_{crit} increases in unit steps with increasing Re_i and the critical Taylor number increases monotonically as Re_i increases away from 0, the current nonisothermal results show that m_{crit} can change by more than one unit, may assume positive and negative values, and that $\overline{\mathrm{Ta}}_{i,\mathrm{crit}}$ is not generally monotonic over the entire range of Re_i considered. As can be seen by comparing Figs. 12 and 13(b), the range of Re_i for which the critical disturbance is axisymmetric is larger for the current nonisothermal results than for the isothermal constant property case, and as shown in Refs. 4–6, 8, 18, 36, and 37, the size of this finite range of Re_i is a very strong function of the radius ratio. As for the critical axial wave number shown in Fig. 13(c), we note that current nonisothermal $\bar{a}_{\mathrm{crit}}$ values can be below or above those of the isothermal constant property case depending on the value of Re_i. In contrast to the other nonisothermal $\bar{a}_{\mathrm{crit}}$ results presented here, for $\Theta_i=1.08$ $\bar{a}_{\mathrm{crit}}$ lies very close to the isothermal constant property results for $\mathrm{Re}_i \leqslant 40$ even though m_{crit} differs greatly. Finally, we note that $\bar{c}_{\mathrm{crit}}$ values for the isothermal constant property case shown in Fig. 13(d) are positive over the entire range of Re_i considered here, whereas in the current nonisothermal work the critical axial wave speed is also positive, but much smaller in magnitude at large Re_i.

Next, we consider the comparison of the current results to the $\mathrm{Re}_i=0$ experimental results of White and Muller.[25,32,38] We note that a detailed comparison has been made in Ref. 28 but because of the discrepancies noted in Sec. III B between the current work and that of Ref. 28 we have decided to reconsider the comparison. In Ref. 28 the authors compare to experimental results for $T_i=291.65$ K for which White and Muller[38] found the critical Taylor number to be 12.75 and the critical frequency to be nonzero (i.e., nonstationary vortices), where for no temperature difference between the cylinder walls Ref. 28 found $\mathrm{Ta}_{i,\mathrm{crit}}=12.61$ and the critical frequency to be 0 (i.e., stationary vortices). The authors in Ref. 28 then went on to postulate that given the experimental setup, there could have been a temperature difference between the cylinder walls, and showed that if one assumed a temperature difference between the cylinder walls of 1 K that the critical Taylor number increased to 14.32 and the critical disturbance was now nonstationary. This discrepancy between computation and experiment (i.e., the numerically computed value being greater than the experimental value) would seem to

suggest that the instability is actually subcritical, and with this in mind Ref. 28 performed time-dependent simulations that also suggested this fact. On the other hand, we use the current results for nonzero axial flow to suggest an alternative mechanism by which the critical disturbance for the case of no temperature difference between the cylinder walls may be nonstationary. As shown by the current results, for nonzero axial flow the critical disturbance is nonstationary (i.e., nonzero frequency). Thus, if there was any amount of axial flow in the experiments this could account for the observed small nonzero critical disturbance frequency. We note that in the current work we have found a critical Taylor number of approximately 10.1 for $\mathrm{Re}_i=0$, and point out that very little axial flow is needed to increase this value to that of the experiments and get a slightly nonzero critical disturbance frequency. Also, we note that previous work[8] has shown that linear stability results for these types of flows are in good agreement with experiment over a large range of parameter space.

C. Instability mechanism

For the case of no axial flow, the instability appears to be due to a coupling between viscous dissipation-induced temperature stratification and centrifugal destabilization as pointed out in Refs. 25, 28, 32, and 38 and also verified by the current results. As for the $\mathrm{Re}_i \neq 0$ results, we see that the addition of axial flow significantly stabilizes the base state, which is consistent with isothermal constant property results.[4–6,8,37] In order to isolate the essential cause of stabilization due to axial flow, critical conditions are recomputed after terms are eliminated from the linearized equations. This process allows identification of the terms proportional to v_{zb} or $\partial v_{zb}/\partial r$ in the disturbance equations that are important. There are five terms in the disturbance equations proportional to these expressions, and we note that all but one have little effect on the critical Taylor number. The one term that does have a significant effect on the critical Taylor number is the expression $v_{zb}(\partial T'/\partial z)$ in the energy disturbance equation, where results show that turning off this term significantly decreases the critical Taylor number (i.e., this term has a stabilizing effect). Results show that the amount of stabilization due to this term is a strong function of the Reynolds number, and that at large Reynolds numbers this term plays less of a role, which might account for the apparent plateau seen in the stability boundaries at large Re_i. Thus, fluctuations in the temperature field created as a result of the coupling between the base flow axial velocity component and the axial derivative of the temperature perturbation play an important role in stabilizing the flow.

VI. CONCLUSIONS

For $\eta=0.827$, linear stability results for circular Couette flow with viscous heating have been presented in Sec. IV, and these results show that the stability boundaries are greatly affected by viscous heating and axial flow. For $\mathrm{Re}_i=0$, results show that $\overline{\mathrm{Ta}}_{i,\mathrm{crit}}$ varies significantly over the temperature range considered, and that there is approximately an order of magnitude difference between the current nonisothermal results and those found for the isothermal constant property case (cf. Ref. 8 for a detailed account of the isothermal results for values of η bounding the current value). Also, we find that for $\mathrm{Re}_i=0$ the critical disturbance is axisymmetric over the entire range of temperatures considered. We note that for $\mathrm{Re}_i=0$, our stability boundaries are qualitatively similar to those found by Al-Mubaiyedh *et al.*[28] but in the current work we show that the magnitude of $\overline{\mathrm{Ta}}_{i,\mathrm{crit}}$ differs between the two works. For $\mathrm{Re}_i \neq 0$, results differ significantly from the $\mathrm{Re}_i=0$ case in that the critical disturbance is no longer purely axisymmetric but is a strong function of Re_i, and unlike the $\mathrm{Re}_i=0$ case considered here and the isothermal constant property case for similar values of η,[8] $\overline{\mathrm{Na}}_{i,\mathrm{crit}}$ is not monotonic over the entire range of Re_i considered. Also, closed disconnected neutral curves have been found for values of η for which no closed disconnected neutral curves have been found in the isothermal case, but we note that they do not lead to multivalued stability boundaries as they do in the isothermal case for smaller values of η (cf. Refs. 6 and 37).

ACKNOWLEDGMENTS

One of the authors (D.L.C.) was supported by a National Research Council Postdoctoral Fellowship, and the other author (G.B.M.) was supported by the Microgravity Research Division of NASA.

[1] G. I. Taylor, "Stability of a viscous liquid contained between two rotating cylinders," Philos. Trans. R. Soc. London, Ser. A **223**, 289 (1923).
[2] R. J. Cornish, "Flow of water through fine clearances with relative motion of the boundaries," Proc. R. Soc. London, Ser. A **140**, 227 (1933).
[3] S. Goldstein, "The stability of viscous fluid flow between rotating cylinders," Proc. Cambridge Philos. Soc. **33**, 41 (1937).
[4] D. I. Takeuchi and D. F. Jankowski, "A numerical and experimental investigation of the stability of spiral Poiseuille flow," J. Fluid Mech. **102**, 101 (1981). corrigendum, *ibid.* **113**, 536 (1981).
[5] B. S. Ng and E. R. Turner, "On the linear stability of spiral flow between rotating cylinders," Proc. R. Soc. London, Ser. A **382**, 83 (1982).
[6] D. L. Cotrell and A. J. Pearlstein, "The connection between centrifugal instability and Tollmien-Schlichting-like instability for spiral Poiseuille flow," J. Fluid Mech. **509**, 331 (2004).
[7] W. H. Reid, "Review of 'The hydrodynamic stability of viscid flow between coaxial cylinders' by S. Chandrasekhar," Math. Rev. **22**, 565 (1961).
[8] D. L. Cotrell, S. L. Rani, and A. J. Pearlstein, "Computational assessment of subcritical and delayed onset in spiral Poiseuille flow experiments," J. Fluid Mech. **509**, 353 (2004).
[9] C. S. Yih, "Dual role of viscosity in the instability of revolving fluids of variable density," Phys. Fluids **4**, 806 (1961).
[10] W. Lai, "Stability of a revolving fluid with variable density in the presence of a circular magnetic fluid," Phys. Fluids **5**, 560 (1962).
[11] K. M. Becker and J. Kaye, "Measurements of diabatic flow in an annulus with an inner rotating cylinder," J. Heat Transfer **84**, 97 (1962).
[12] J. Walowit, S. Tsao, and R. C. DiPrima, "Stability of flow between arbitrary spaced concentric cylindrical surfaces including the effect of radial temperature gradient," J. Appl. Mech. **31**, 585 (1964).
[13] C. H. Kong and I. C. Liu, "The stability of nonaxisymmetric circular Couette flow with a radial temperature gradient," Phys. Fluids **6**, 2617 (1994).
[14] V. M. Soundalgekar, H. S. Takhar, and T. J. Smith, "Effects of radial temperature gradient on the stability of a viscous flow in an annulus with a rotating inner cylinder," Waerme- Stoffuebertrag. **15**, 233 (1981).
[15] H. S. Takhar, T. J. Smith, and V. M. Soundalgekar, "Effects of radial temperature gradient on the stability of a viscous incompressible fluid between two rotating cylinders," J. Math. Anal. Appl. **111**, 349 (1985).

[16]J. C. Chen and J. Y. Kuo, "The linear stability of steady circular Couette flow with a small radial temperature gradient," Phys. Fluids A **2**, 1585 (1990).
[17]H. S. Takhar, V. M. Soundalgekar, and M. A. Ali, "Effects of radial temperature gradient on the stability of a narrow-gap annulus flow," J. Math. Anal. Appl. **152**, 156 (1990).
[18]D. L. Cotrell and G. B. McFadden, "Linear stability of spiral Poiseuille flow with a radial temperature gradient: Centrifugal buoyancy effects," Phys. Fluids **17**, 114102 (2005).
[19]I. S. Bjorklund and W. M. Kays, "Heat transfer between concentric rotating cylinders," J. Heat Transfer **81**, 175 (1959).
[20]F. C. Haas and A. S. Nissan, "Experimental heat transfer characteristics of a liquid in Couette motion and with Taylor vortices," Proc. R. Soc. London, Ser. A **261**, 215 (1961).
[21]C. Y. Ho, J. N. Nardacci, and A. H. Nissan, "Heat transfer characteristics of fluids moving in a Taylor system of vortices," AIChE J. **10**, 194 (1964).
[22]H. A. Snyder and S. K. F. Karlsson, "Experiments on the stability of Couette motion with a radial thermal gradient," Phys. Fluids **7**, 1696 (1964).
[23]M. M. Sorour and J. E. R. Coney, "The effect of temperature gradient on the stability of flow between vertical, concentric, rotating cylinders," J. Mech. Eng. Sci. **21**, 403 (1979).
[24]M. Ali and P. D. Weidman, "On the stability of circular Couette flow with radial heating," J. Fluid Mech. **220**, 53 (1990).
[25]J. M. White and S. J. Muller, "Experimental studies on the stability of Newtonian Taylor-Couette flow in the presence of viscous heating," J. Fluid Mech. **462**, 133 (2002).
[26]A. A. Kolyshkin and R. Vaillancourt, "On the stability on non-isothermal circular Couette flow," Phys. Fluids A **5**, 3136 (1993).
[27]U. A. Al-Mubaiyedh, R. Sureshkumar, and B. Khomami, "Influence of energetics on the stability of Taylor-Couette flow," Phys. Fluids **11**, 3217 (1999).
[28]U. A. Al-Mubaiyedh, R. Sureshkumar, and B. Khomami, "The effect of viscous heating on the stability of Taylor-Couette flow," J. Fluid Mech. **462**, 111 (2002).
[29]D. G. Thomas, R. Sureshkumar, and B. Khomami, "Influence of fluid thermal sensitivity on the thermo-mechanical stability of the Taylor-Couette flow," Phys. Fluids **15**, 3308 (2003).
[30]P. C. Sukanek, C. A. Glodstein, and R. L. Laurence, "The stability of plane Couette flow with viscous heating," J. Fluid Mech. **57**, 651 (1973).
[31]P. C. Sukanek and R. K. Laurence, "An experimental investigation of viscous heating in some simple shear flows," AIChE J. **20**, 474 (1974).
[32]J. M. White and S. J. Muller, "The role of thermal sensitivity of fluid properties, centrifugal destabilization, and nonlinear disturbances on the viscous heating instability in Newtonian Taylor-Couette flow," Phys. Fluids **14**, 3880 (2002).
[33]J. R. A. Pearson, "Polymer flows dominated by high heat generation and low heat transfer," Polym. Eng. Sci. **18**, 222 (1978).
[34]E. A. Kearsley, "The viscous heating correction for viscometer flows," Trans. Soc. Rheol. **6**, 253 (1962).
[35]A. J. Kearsley, "A steady state model of Couette flow with viscous heating," Int. J. Eng. Sci. **32**, 179 (1994).
[36]A. Meseguer and F. Marques, "On the competition between centrifugal and shear instability in spiral Poiseuille flow," J. Fluid Mech. **455**, 129 (2002).
[37]D. L. Cotrell and A. J. Pearlstein, "Linear stability of spiral and annular Poiseuille flow for small radius ratio," J. Fluid Mech. **547**, 1 (2006).
[38]J. M. White and S. J. Muller, "Viscous heating and the stability of Newtonian and viscoelastic Taylor-Couette flows," Phys. Rev. Lett. **84**, 5130 (2000).